International Journal of Solids and Structures 271–272 (2023) 112259

Contents lists available at ScienceDirect

International Journal of Solids and Structures

journal homepage: www.elsevier.com/locate/ijsolstr

Mechanical behaviour of rubber blocks

Alessandra Orfeo [a,*], Enrico Tubaldi [a], Alan H. Muhr [b]

[a] Department of Civil and Environmental Engineering, University of Strathclyde, Glasgow, UK
[b] Tun Abdul Razak Research Centre-TARRC, Hertford SG13 8NL, UK

ARTICLE INFO

Keywords:
Rubber blocks
FE models
Low shape factor
Coupled horizontal-vertical behaviour

ABSTRACT

This study investigates the behaviour of rubber blocks bonded between two plates under combined compression and shear loading, using experimental and numerical analyses, and also approximate analytical theories. First, experimental data from a series of compression and shear tests of rubber blocks with different aspect ratios are presented. Next, numerical simulations are carried out with three-dimensional finite element (FE) models, allowing insight to be gained into the stress and strain fields within the blocks. Existing analytical theories for blocks under compression and combined compressive and shear loading are then reviewed, and their accuracy is evaluated against test and numerical results. The study shows that those theories accounting for the effect of the axial shortening of the blocks provide a better description of the combined compression and shear behaviour, compared to theories, developed for laminated structural bearings with many thin rubber layers, that ignore this effect. An improved theory is also proposed, which better describes the effects of the bulging of the compressed blocks on their shear and flexural parameters and provides a better fit to experimental and numerical results.

1. Introduction

Rubber pads or blocks have been widely employed for more than a century in numerous applications, e.g. as springs, elastic joints or isolators in structures or mechanical systems, as frictional liners in contact with substrates, and for energy dissipation. The shapes, mechanical properties and chemical composition of the blocks are designed to achieve the performance required by the particular service condition. Usually, the rubber is faced at the mounting surfaces with bonded metal plates; rough contact surfaces such as concrete may also suppress lateral spreading of the rubber when compressed. When lateral spread at the contact surfaces is suppressed, we may define the (primary) shape factor S of a rubber pad or block as the ratio of the loaded area at one end face to the unloaded area of the sides, these being free to bulge when the pad is compressed.

For some applications, a high shape factor is desirable, and may be achieved by laminating the rubber with an appropriately large number of reinforcing steel plates, so that each rubber layer has a high shape factor, resulting in high axial stiffness (i.e. in the direction normal to the steel plates). In other applications the use of lower shape factors may be preferred (Orfeo et al. 2022). For example, bridge bearings with relatively low shape factor can better accommodate rotations compared to high shape factor bearings. Low shape factor blocks have been used as vibration isolation mounts for equipment, combined shear and compression mounts for car engines and transmissions, and as suspension springs for rail vehicles and heavy goods road vehicles, typically as multilayer laminates with a shape factor of each layer of the order of 1 (e.g. Hirst, 1961).

Low shape factor (LSF) blocks have interesting characteristics for seismic isolation of structures. The first building to be isolated on rubber bearings, the Pestalozzi school in Skopje, Macedonia, was mounted on unreinforced elastomeric LSF blocks ($S = 0.5$), a design stemming from prior experience of mounting systems for imparting blast resistance to military structures (Siegenthaler, 1970). More usually, LSF rubber bearings consist of a few rubber layers of moderate thickness sandwiched between, and bonded to, steel plates to increase the stiffness in the direction normal to the plates (Aiken et al. 1989). Thus, they might constitute a cost-effective solution for providing isolation for ground-borne vibration or three-dimensional seismic isolation of structures. The process needed to produce rubber bearings requires many steps from initial conception (assembling, vulcanization) to final installation, and assembling fewer steel and rubber layers to form LSF bearings can save time and costs, lower the risk of defects during the production process, and also reduce the weight of the bearings, making them easier to manhandle.

Many experimental and analytical studies since the early 1960 s have

* Corresponding author.
E-mail address: alessandra.orfeo@strath.ac.uk (A. Orfeo).

https://doi.org/10.1016/j.ijsolstr.2023.112259
Received 29 August 2022; Received in revised form 14 February 2023; Accepted 6 April 2023
Available online 11 April 2023

focused on the characterization of the behaviour of rubber blocks and laminated bearings under compressive loading and under combined vertical and horizontal loading. A theory was developed by Haringx (1948, 1949a, 1949b, 1949c) considering a shear-flexible column, and applied to rubber rods with no reinforcing plates. Gent (1964) adapted this model to study the elastic stability of multilayer laminated rubber bearings and the reduction of their horizontal stiffness for increasing axial loads. Experimental tests on the behaviour of cylindrical rubber blocks under combined vertical and horizontal loading were also carried out by Payne (1962), who provided a validation of the theory of Haringx in the case of low shape factors, between 0.08 and 2.2. The dynamic shear experiments of Howgate (1979) were the first to highlight an interesting aspect of the mechanical behaviour of rubber blocks, which exhibit an increase in hysteresis and non-linearity under horizontal forces when compressed by increasing axial loads approaching the critical load for stability. The behaviour of laminated rubber bearings continued to be the subject of many experimental and analytical studies in the subsequent decades up to date (see e.g. Warn (2014) for a review of the most important ones, including the Koh and Kelly model (1988), widely used for seismic isolation bearings).

Although these theories and models stemming from the original formulations of Gent (1964), Thomas (1982) and Koh and Kelly (1988) can be used to describe the behaviour of multilayer laminated bearings with moderately high shape factors, they are not suitable for the case of LSFs, whether laminated or as single rubber blocks. Indeed, apart from the initial application of the theory by Haringx (1949a, 1949b, 1949c) to rubber rods, the focus was on high shape factors ($1 \ll 2S^2$), and on the correction for a finite bulk modulus K which becomes significant if the assumption that $6GS^2 \ll K$, is not justifiable, corresponding to $S > 10$ (e.g. Chalhoub & Kelly, 1990, and some papers reviewed by Roeder et al (1987)). In contrast, for LSF bearings, we cannot disregard important effects such as the reduction in height and the increase in plan area due to bulging of the elastomer under compressive load (Stanton et al., 1990; Muhr, 2017; Schapery, 2018). Few experimental studies have focused specifically on LSF rubber blocks. Fan et al. (1992) carried out experimental tests on quadruple shear assemblies made with blocks with S values below 1.5. The assemblies were tested by varying the horizontal displacements at each of several fixed vertical compressions. Cilento et al. (2017) conducted further experiments on LSF rectangular and cylindrical blocks. Experimental tests on multilayer laminated bearings are numerous (e.g. Aiken et al. 1989, Yabana and Matsuda, 2000, Cardone and Perrone, 2012), though mainly focused on S values higher than 5.

Some analytical formulations were specifically developed for LSF rubber blocks and bearings. Among these, Roeder et al. (1987) and Stanton et al. (1990), proposed to take into account the effect of axial shortening due to compression on the shear and bending stiffnesses. Their theory was also validated by experimental tests demonstrating that bearings with a height-to-width ratio below a certain limit do not become laterally unstable under any axial load. Lanzo (2004) took into account the axial stiffness of rubber bearings, considering both a linear elastic and a hyperelastic constitutive model for the rubber. Muhr (2017) also developed a theory for the lateral stiffness of single layer blocks of rubber with bonded endplates under finite axial deformation, based on the work of Goodchild et al. (2018) on the lateral stiffness and damping of stretched rubber beams. A comparison of these theories and an in-depth assessment of their accuracy has never been carried out to date.

This paper investigates, with theoretical and numerical tools, the behaviour of low-damping LSF rubber blocks under combined vertical and horizontal loading. In particular, the blocks tested experimentally by Fan et al. (1992) are considered. Different numerical models, developed in ABAQUS (‘Dassault Systèmes, 2018) considering various constitutive laws, are employed to simulate these tests. They are also used to gain an insight into the internal distribution of stress and strain within the bearings due to the application of the external boundary conditions, and to evaluate the influence of the models used to describe the rubber constitutive behaviour on the horizontal force–displacement behaviour of the compressed blocks. The accuracy of various analytical theories for the evaluation of the horizontal stiffness and the critical load of bonded LSF blocks is assessed. An extended theory, accounting for the non-uniform bulging along the compressed rubber block, is also proposed.

Section 2 of the paper describes the experimental campaign at TARRC carried out by Fan et al. (1992). In Section 3, the numerical simulations of the tests are illustrated, whereas in Section 4 the accuracy of the various analytical models considered is evaluated. The paper ends with a conclusion section, where future studies are also discussed.

2. Experimental campaign

The tests considered in this study are those described also in Fan et al. (1992) and were performed at the Tun Abdul Razak Research Centre (TARRC) on rectangular rubber blocks. An unfilled natural rubber mix was employed to make the samples and the compound recipe is SMR5, 100; ZnO, 5; stearic acid, 2; sulphur 2.5; CBS, 0.6; Santoflex 13, 2; where the numbers are parts by weight. Both ends of each block were bonded to metal plates using the Chemlok 205/220 system. The dimensions and shape factors of the rubber blocks are given in Table 1 where h_0, a_0 and b_0 are the undeformed rubber height, minimum width and maximum width respectively. The top and bottom metal plates share the rubber width dimension (e.g. see Block B in Fig. 1a), except for Block X, which has oversized plates, i.e. 50 mm, as shown in Fig. 1b.

A quadruple shear apparatus was used for the force–deformation experiments, as shown in Fig. 2a. The rectangular blocks were sheared in the direction normal to side b_0, their longest plan dimension, this being the direction of lowest stability. A 100kN Instron universal test machine (model 1115) was used to achieve the desired compression, and then shear deflections were achieved by hand adjustment of a lead screw (D in Fig. 2a), threaded through the steel block separating the righthand pair of bonded rubber blocks, and able to control the relative separation of the two stacks at their midheight for either sign of lateral force, measured by the load cell B. It was initially assumed that the shear deflections would remain equal and opposite for the two stacks of blocks, so that the turns on the lead screw could be used to determine the lateral deflection at the mid height of each stack. However, the mid-height plane of the apparatus is free to toggle to any position where the lateral force applied between the stacks is in balance, and at high loads their deflections are not necessarily equal and opposite. To determine the lateral deflection of each individual bearing, a dial gauge attached to the Instron crosshead was introduced. The two lateral deflections could then be calculated from the dial gauge reading plus the differential deflection determined from the lead screw. A shear force–deflection curve with little hysteresis was found when the block was subjected to shear deflection while keeping the compressive deflection constant and small, as shown in Fig. 2b for a compression of 5.4 mm. However, for a compressive deflection exceeding instability there was a large spontaneous shear deflection, although this was observed to take place over several seconds, suggestive of a viscoelastic relaxation process. The shear force–deflection curve shown in Fig. 2b for a compression of 9.4 mm reveals a large hysteresis. As the compound chosen for the testpieces

Table 1
Rubber blocks geometry.

Block	h_0	a_0	b_0	$S = \frac{a_0 b_0}{(2a_0 + 2b_0)h_0}$
	mm	mm	mm	-
B	10	54	66.5	1.49
C	20	53.5	66.5	0.74
D	30	53.5	66	0.49
X	77.5	34	64	0.14

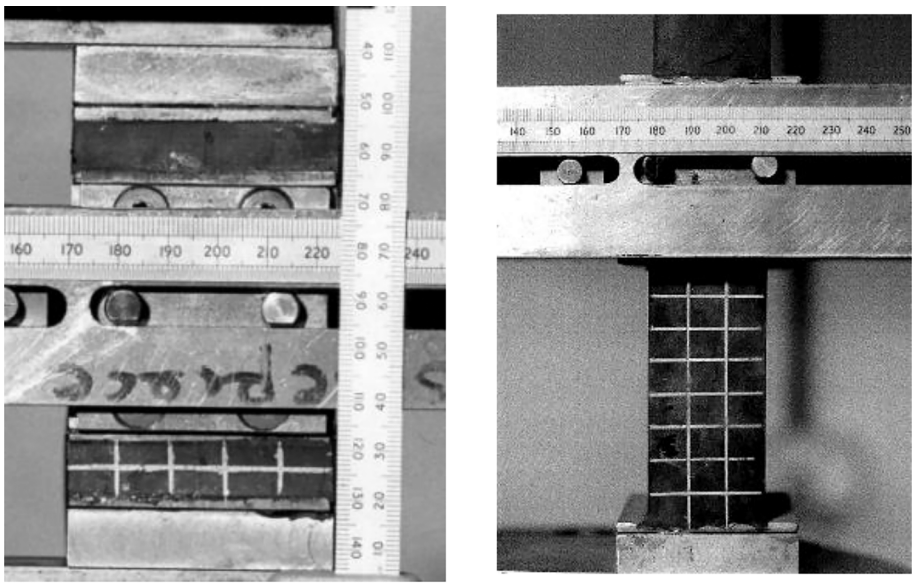

Fig. 1. Details of two blocks used during for the experimental tests (a) Block B (b) Block X.

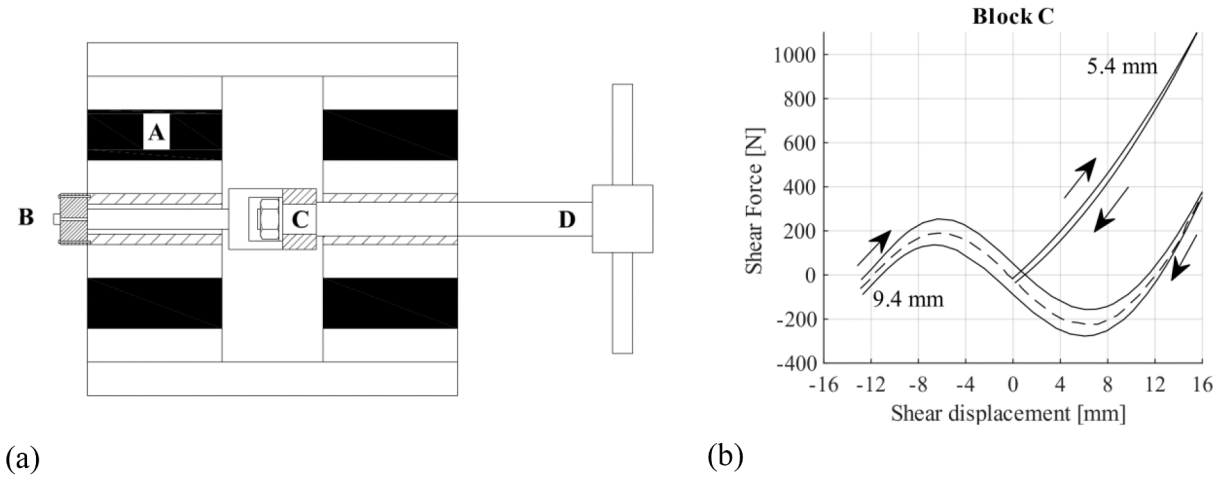

Fig. 2. (a) Quadruple shear apparatus (b) Typical shear-deflection plots (source:block C at vertical deflections of 5.4 mm and 9.4 mm, Fan et al., 1992).

is a low-damping one, this observation may seem puzzling, but is a consequence of the very high strain energy throughout the rubber, and the low magnitude of lateral elastic stiffness under this deformation, making the viscous part of its viscoelastic nature more evident. Reference can be made to Orfeo et al. (2022) for further insight into this phenomenon. A mean curve for the pair of blocks (the dashed line in Fig. 2b) showing the large excursion in shear was constructed and taken as the experimental shear force–deflection curve.

3. Numerical modelling and comparison with experimental results

3.1. FE models

This section describes the three-dimensional FE models developed in ABAQUS (Dassault Systèmes 2018) to simulate the tests on the LSF blocks. Only half of each block is modelled, thanks to symmetry. Fig. 3 shows the blocks meshed using solid C3D8R elements, which are 8-node linear elements with reduced integration. Geometric non-linearities are taken into account in the analysis. Blocks B, C and D have a mesh finer toward the free rubber surface, where the strain gradients are highest. Block X has all elements with the same approximate global size. Moreover, the model of Block X includes the steel end plates meshed using C3D8R elements and connected to the rubber block using tie constraints. Refining further the meshes does not affect the global force–displacement response of the bearings, nor the strains and stresses far from critical locations at the boundaries, where singularities are expected.

In ABAQUS (Dassault Systèmes 2018), the following strain energy function is used for modelling rubber materials:

$$U = \sum_{i=1}^{N} \frac{2\mu_i}{\alpha_i} \left[\lambda_1^{\alpha_i} + \lambda_2^{\alpha_i} + \lambda_3^{\alpha_i} - 3\right] + \sum_{i=1}^{N} \frac{1}{D_i}(J-1)^{2i} \tag{1}$$

where U is the strain energy per unit of reference volume, λ_i are principal stretches, J is the ratio of current to original volume, the parameters μ_i and α_i control the deviatoric behaviour of the material, while the constant D_i characterize the volumetric behaviour (compressibility).

Two different constitutive models are considered in the FE analyses,

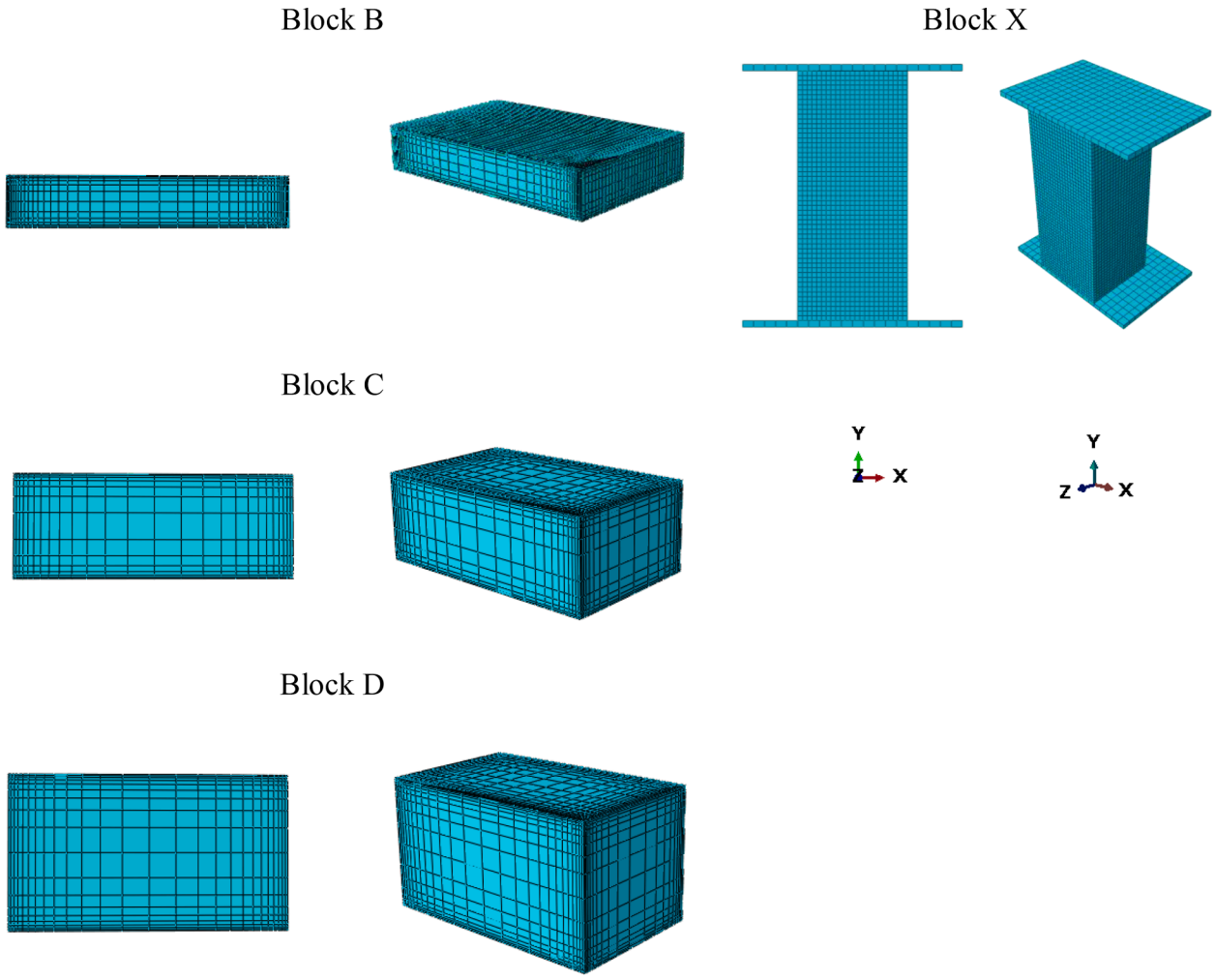

Fig. 3. Finite element model of the rubber blocks: Front and 3D view.

with the aim of investigating the influence of the rubber constitutive model on the simulation of the behaviour of the blocks. The first one is an Ogden model, with $N = 1$, $\mu_1 = 0.478$ MPa, $\alpha_1 = 2.3$, $D_1 = 0.0001$ $N^{-1}mm^2$ (corresponding to a bulk modulus of $K = 2000$ MPa). The values of $\mu_1$and α_1 for this model have been chosen to provide the best fit to all the experimental tests carried out on the blocks. The second model considered is a simpler, neo-Hookean constitutive model, corresponding to $N = 1$, $\mu = 0.5$ MPa, $\alpha = 2$ and $D_1 = 0.0001$ $N^{-1}mm^2$.

The behaviour of the constitutive rubber models in uniaxial compression and tension is shown in Fig. 4a-b in terms of nominal stresses, i.e. ratio of force to unloaded area, versus λ_1,. Fig. 4c shows the rubber behaviour in simple shear configuration in terms of shear stresses - shear strain γ. Fig. 4d shows the variation with λ_1 of the strain energy density function of the Ogden and neo-Hookean constitutive models in both uniaxial tension and simple shear configurations. The two material models exhibit a similar behaviour under the various deformation modes only at small strains, while at large strain the Ogden model is stiffer in shear and tension, and slightly softer in compression. It is noteworthy that under vertical and horizontal loading, the rubber blocks are subjected to a complex state of deformation, involving compressive, shear and even tensile strains.

The numerical simulations of the quasi-static tests on the rubber blocks are carried out using a dynamic explicit solution algorithm, in order to overcome some difficulties in achieving convergence in the analyses of highly compressed and sheared blocks. The choice of the time step size Δt is very critical in this type of explicit analysis, since small-time increments need to be used to achieve stable and accurate results. An approximate estimate of the limit value $\Delta t_{\max}$ of the time increment ensuring stability is given by the smallest transit time of a dilation wave across any of the element in the mesh (Dassault Systèmes 2018):

$$\Delta t_{\max} = \frac{L_{\min}}{c_d} \tag{2}$$

where $L_{\min}$ is the smallest element dimension in the mesh and c_d is the wave speed of the material, which in the case of a linear elastic material can be expressed as follows:

$$c_d = \sqrt{\frac{E}{\rho}} \approx \sqrt{\frac{1.5MPa}{967kg/m^3}} \approx 39ms^{-1} \tag{3}$$

where E is the Young's modulus and ρ the density. Applying Equations (2) and (3) to the problem at hand, very small values of $\Delta t_{\max}$ are obtained. Thus, a mass scaling factor of 10^{-5} was used to increase the time step size and reduce the computational burden of the analyses. At the end of each analysis, a check was made that the value of the ratio of the kinetic energy to the total energy in the system was less than 4%. It is noteworthy that using an implicit solution algorithm the analyses would not converge in many cases.

With regards to the boundary condition of the blocks, the displacements and rotations along the x-, y- and z- directions of the bottom surface were constrained for all the tests. The out of plane displacement along z and rotation about $\times$ and y of the nodes lying on the $z = 0$ plane

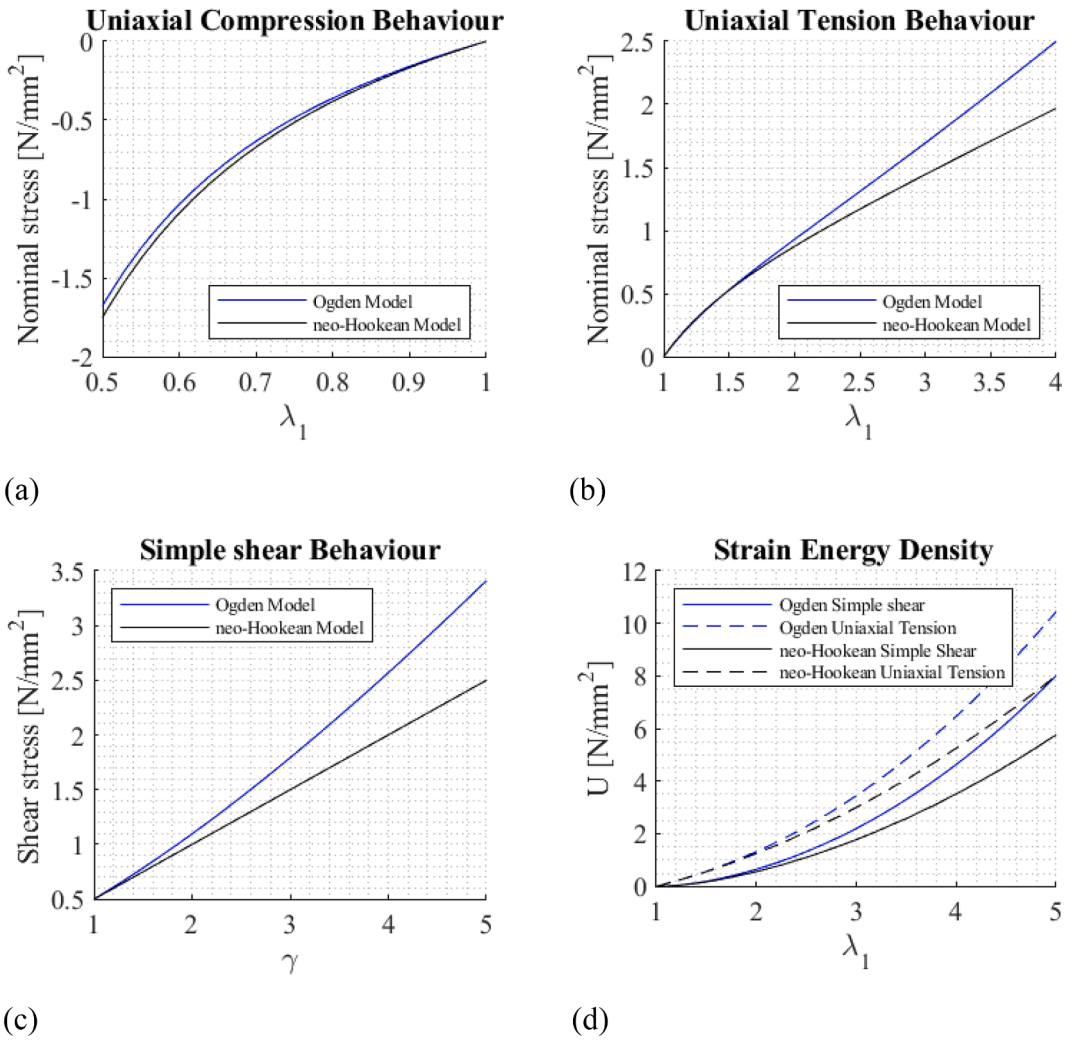

Fig. 4. Comparison of Ogden and neo-Hookean constitutive models under (a) uniaxial compression, (b) uniaxial tension $\lambda_2 = \lambda_3$ and (c) simple shear $\lambda_2 = 1$. (d) Strain Energy Density function in uniaxial tension and simple shear configuration.

are restrained to account for symmetry. Finally, only displacement along *x*- and *y*- are allowed on the top surface. In the experiments, vertical displacements were first imposed on the top surface of the blocks. Subsequently horizontal differential displacements were applied, while preventing vertical motion and rotation of the top surface.

3.2. FE analysis results

Table 2 reports the experimental values of vertical and horizontal displacements applied for each block, which were also used as the FEA inputs. Table 2 also reports, for each block, the values of the nominal axial and shear strains, obtained by dividing respectively the maximum vertical and horizontal displacement by the rubber block height. The vertical and horizontal experimental reaction forces obtained at the end of the application of the maximum vertical and horizontal displacements are also reported, together with the corresponding nominal stresses, obtained by dividing these forces by the initial area A_0 of the transverse section of each rubber block. These values are considered as references to understand the extent of local variations in the stress and strain contours. The "nominal true stresses" given in Table 2 are calculated in a similar way to the "nominal stresses", except that they are based on the deformed area, defined as:

$$A = A_0/\lambda \tag{4}$$

where λ is the axial compression of the block.

Fig. 5 and Fig. 6 give contour plots of local compressive and shear strains respectively for each block subjected to the highest displacements applied. These plots were evaluated considering the Ogden constitutive model for the rubber. It is noteworthy that using a different mesh could lead to significant changes in the local strain and stresses close to the border of the block. This issue is not investigated in this paper. Under compression, in Block X, it can be noted that there is a significant variation of the axial deformations along the rubber height but not along the rubber width, apart from the corners. In blocks B, C and D the bulging is more evident than in Block X, and the maximum compressive and shear strain values are concentrated along the corners. Under shear loading, tensile strains are developed at the top right and bottom left areas of the blocks and there is concentration of compressive strains along a diagonal band, corresponding to the formation of a compression strut. Kalfas et al. (2017) found a similar behaviour in the case of a laminated bearing with the upper plate restrained against rotation. In addition, bending deformation is predominant in block X, as witnessed by the increasing tilt, from the ends towards the midheight cross-section, of the originally horizontal mesh lines, whereas in block B, characterized by the highest shape factor, shear deformation predominates in the core of the block, the originally horizontal mesh lines remaining horizontal, accompanied by bulging on the side. A combination of shear and bending deformation can be observed in C and D. It is also worth noting that the transverse sections stay horizontal in the

Table 2
Experimental data reported by Fan et al. (1992).

	Block B	Block C	Block D	Block X
S [-]	1.49	0.74	0.49	0.14
h_0 [mm]	10	20	30	77.5
Vertical displacements [mm]	0, 3.2, 3.8, 4	0, 5.3, 6.8, 8.2, 9.4	0, 8, 12, 15	0, 5.99, 8.97, 11.94, 13.42, 14.89
Maximum horizontal displacement [mm]	7	17	25	36
Nominal axial strain at max compression [-]	0.4	0.47	0.5	0.19
Nominal shear strain at max. shear [-]	0.7	0.85	0.83	0.47
Vertical reaction force at max compression and zero shear [N]	30,130	13,191	8852	944
Horiz. reaction force at max shear and max compr force [N]	275	505	351	33
Nominal axial stress at max. compression [N/mm^2]	8.39	3.71	2.51	0.43
Nominal true axial stress at max. compression [N/mm^2]	5.03	1.97	1.25	0.35
Nominal shear stress at max shear and max compr. force [N/mm^2]	0.08	0.14	0.10	0.015
Nominal true shear stress at max shear and max compr. force [N/mm^2]	0.046	0.075	0.050	0.012

middle of blocks B, C and D, whereas in the central part of the Block X they are almost perpendicular to the deformed axial centreline, again demonstrating the high contribution of bending deformations.

The local distribution of Cauchy compressive and shear stress within the blocks is similar to that of the strains, and thus is not reported due to space constraints.

Fig. 7 illustrates the contour plot of the total strain energy densities of the elements of each block subjected to the highest vertical compression and horizontal displacement applied in each test. It can be observed that the local strain energy densities increase with increase of the shape factor and thus they are the highest in Block B.

It is noted that the stress and strain concentrations occur at the edges of the plates bonded to the rubber; this is a well-known issue to designers of rubber components, and is mitigated by introducing filets in these regions. The detailing of such designs can be guided by FEA, as discussed by Gough and Muhr (2005).

3.3. Comparison of numerical and experimental results

Fig. 8 shows the variation of the vertical force during compression of the blocks against the vertical deflection according to the experimental results and the FE analyses for the two rubber models. The trend of increase of the compressive forces with the increase of vertical displacement has a rising rate, due to the nonlinear hyperelastic behaviour of the rubber (Fig. 4b), the increase of rubber area due to the bulging of the block, and the approach towards a limiting compression equal to the height of the block, when the tangent stiffness would be infinite. Overall, the compressive behaviour is moderately well described by both material models. The response for the neo-Hookean model is stiffer than that of the Odgen model in the case of Block X, as is also the case in homogeneous compression (Fig. 4a). On the other hand, Blocks B, C and D are characterized by high local shear strains due to the bulging, even under compression, and thus the shear behaviour significantly affects the response. Fig. 4c shows that the behaviour of the neo-Hookean model in simple shear is softer than that of the Ogden model, which is consistent with the softening behaviour particularly evident in Block B for the neo-Hookean material model. Because the forces are much higher for block B, and its initial height is low, accurate displacement measurements during tests on it were more challenging, and in particular the compliance of the test machine might have resulted in the deflection being overestimated. Similarly, the very high stresses and strains may also impair the accuracy of the FEA.

Fig. 9 shows the variation of the compressive force for increasing values of the shear displacement according to the experiments and the FE models. In general, it can be observed that the compressive force reduces with shear deflection. This is related to the well known observation that shear displacement under constant vertical load is accompanied by a decrease in height of rubber bearings. Since this drop in height is prevented by the vertical restraint, the compressive loads decrease with increase in shear. For sufficiently low vertical displacement values, both FEA models describe well the compressive and coupled compressive-shear behaviour of blocks. With the increasing of vertical displacement (i.e. from 11.94 mm for Block X, from 3.8 mm for Block B, from 6.8 mm for block C and from 12 mm for block D), a less good agreement is observed between the FEA results and the experimental results. Using the Ogden material model for the rubber, better results are obtained compared to those obtained using the neo-Hookean model. It is worth noting that the Ogden material model gives higher compressive forces than the neo-Hookean model for all shear displacement values and for all blocks, except for Block X. This can be explained by the fact that in Block X the state of deformation is closer to homogenous compression, under which the Ogden model is softer than the neo-Hookean model (Fig. 4a).

Fig. 10 shows the shear load–deflection curves obtained for different fixed vertical compressions of the blocks. In general, by increasing the vertical displacement, the horizontal stiffness reduces, in line with other studies on the coupled compression-shear behaviour of rubber bearings (Thomas, 1982; Koh and Kelly, 1988). A horizontal tangent marks the condition of instability for the blocks for zero shear displacements. In the case of small compressions, the shear forces exhibit an almost linear trend of increase for increasing shear displacement, whereas under large compression the shear behaviour is highly nonlinear. The FEA model predictions are in good overall agreement with the experiments, with the Ogden model providing the best fit to the test results. The differences between the results obtained with the two different constitutive models are higher for higher compression levels and shear deflections, and the accuracy of the neo-Hookean model reduces significantly for very high values of the compressive displacement. It is also interesting to note that only in the case of shear of the shorter blocks (B,C,D) there is much difference between the FEA models. This can be explained by observing in Fig. 5 and Fig. 6, that local strains and stresses are higher for these blocks than for Block X when the maximum compressive displacement is considered, and that the two hyperelastic constitutive models are very different only at high shear strains (see Fig. 4). It is also interesting to observe that in the case of blocks B, C and D, the response obtained with the neo-Hookean model is stiffer than that obtained with the Ogden model for low compression levels, and more flexible for high compression levels. The opposite trend is observed for Block X.

In order to shed further light into the influence of the compression of the blocks on the shear behaviour, the values of the tangent shear stiffness at zero shear strain according to the FE model and experimental results are calculated and plotted in Fig. 11 vs. the values of the applied vertical deflection. A progressive reduction of the tangent stiffness is observed with increase of the vertical displacement. The results of FEAs show that both material models can reproduce the response of the blocks in terms of shear stiffness versus the axial deflection, and thus also the critical load, to a fair approximation, except for Block B for which the neo-Hookean material model provides very inaccurate estimates when there is significant compression. This can be explained by the fact that the Ogden model is stiffer than the neo-Hookean model under simple shear at very high strains (see Fig. 4).

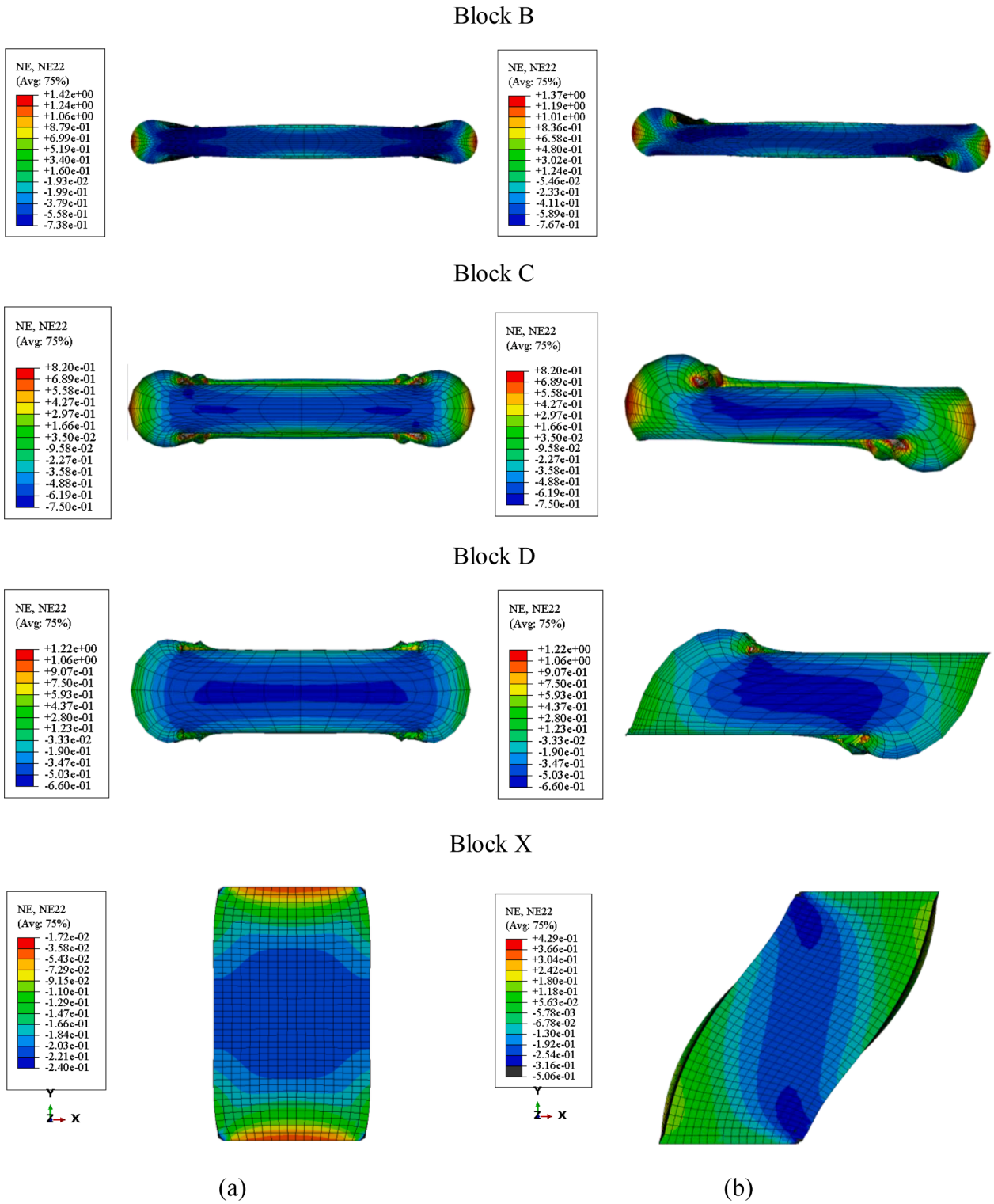

Fig. 5. Contour plot of NE22, i.e. nominal (i.e. engineering) compressive strains along Y direction, for half blocks subjected to (a) maximum compressive displacement alone and (b) maximum compressive displacement in combination with horizontal displacement.

4. Analytical modelling and comparison with experimental and numerical results

In this section, the theories proposed over the years for describing the compressive behaviour of rubber blocks of any aspect ratio are tested against the experimental and numerical results presented in the previous section. An extended theory, informed by the FE analyses results, is also proposed to take into account the non-uniform bulging along the compressed rubber block in the evaluation of the horizontal response of compressed blocks. Finally, analytical and numerical predictions of critical loads are compared with the experimental results.

4.1. Compression behaviour

Haringx (1948, 1949a, 1949b), developed load-compression relationships for the case of bonded rubber blocks using Kosten (1942)

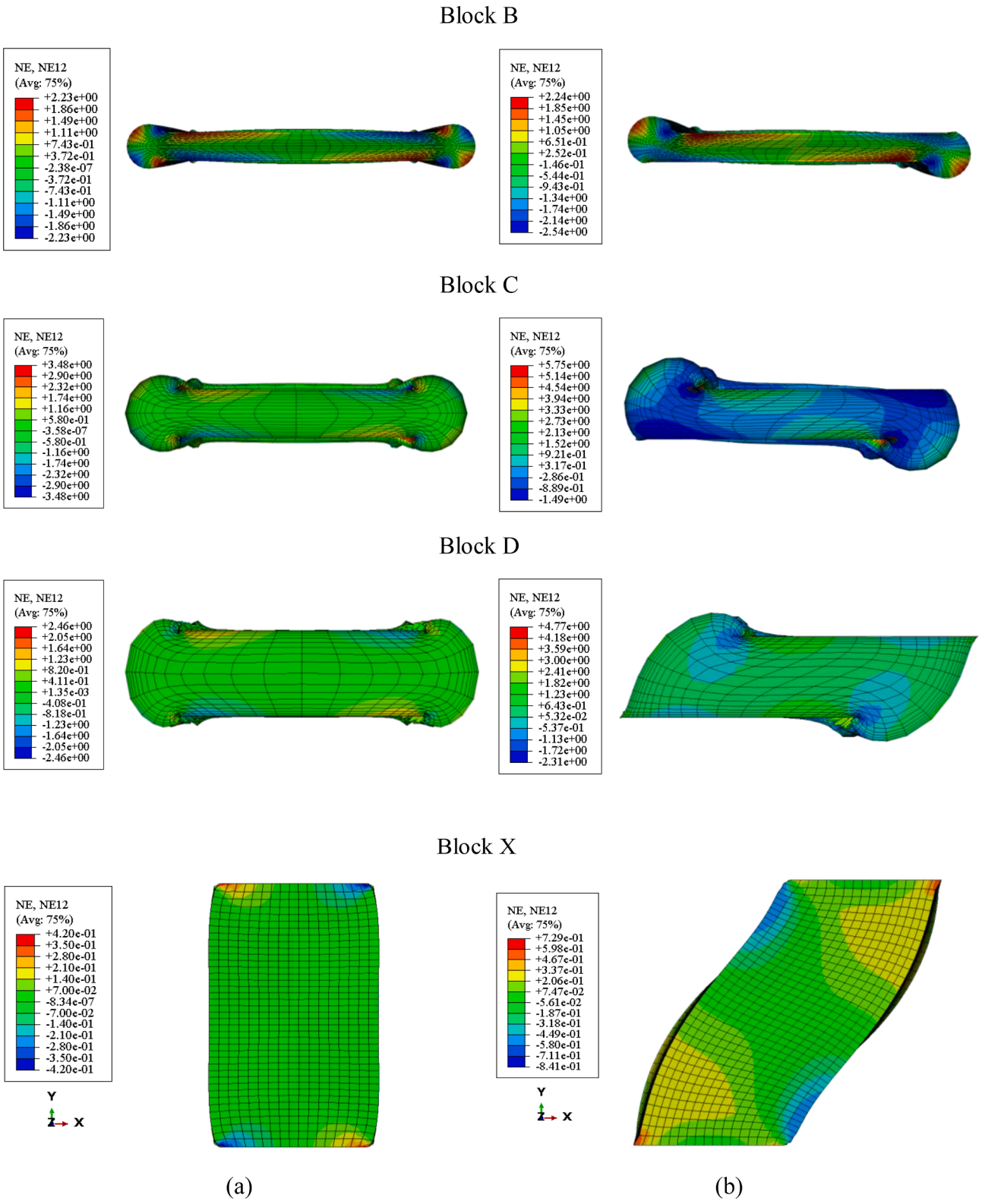

Fig. 6. Contour plot of N12, i.e. nominal (i.e. engineering) shear strain distribution in the shear plane XY for half blocks subjected to (a) maximum compressive displacement alone and (b) maximum compressive displacement in combination with horizontal displacement.

boundary condition at the rubber ends: 1) unrestrained shear behaviour up to the bonded surface and 2) a fraction of the total rubber height equal to 1/8 of the shortest side of a rectangular block is assumed rigid to compression and (presumably) tilt. The compression load–displacement of the remainder of the block was taken as proportionality between true axial stress and strain, giving:

$$N = 3G\frac{A_0}{\lambda^{*2}}(1-\lambda^{*}) \tag{5}$$

Where

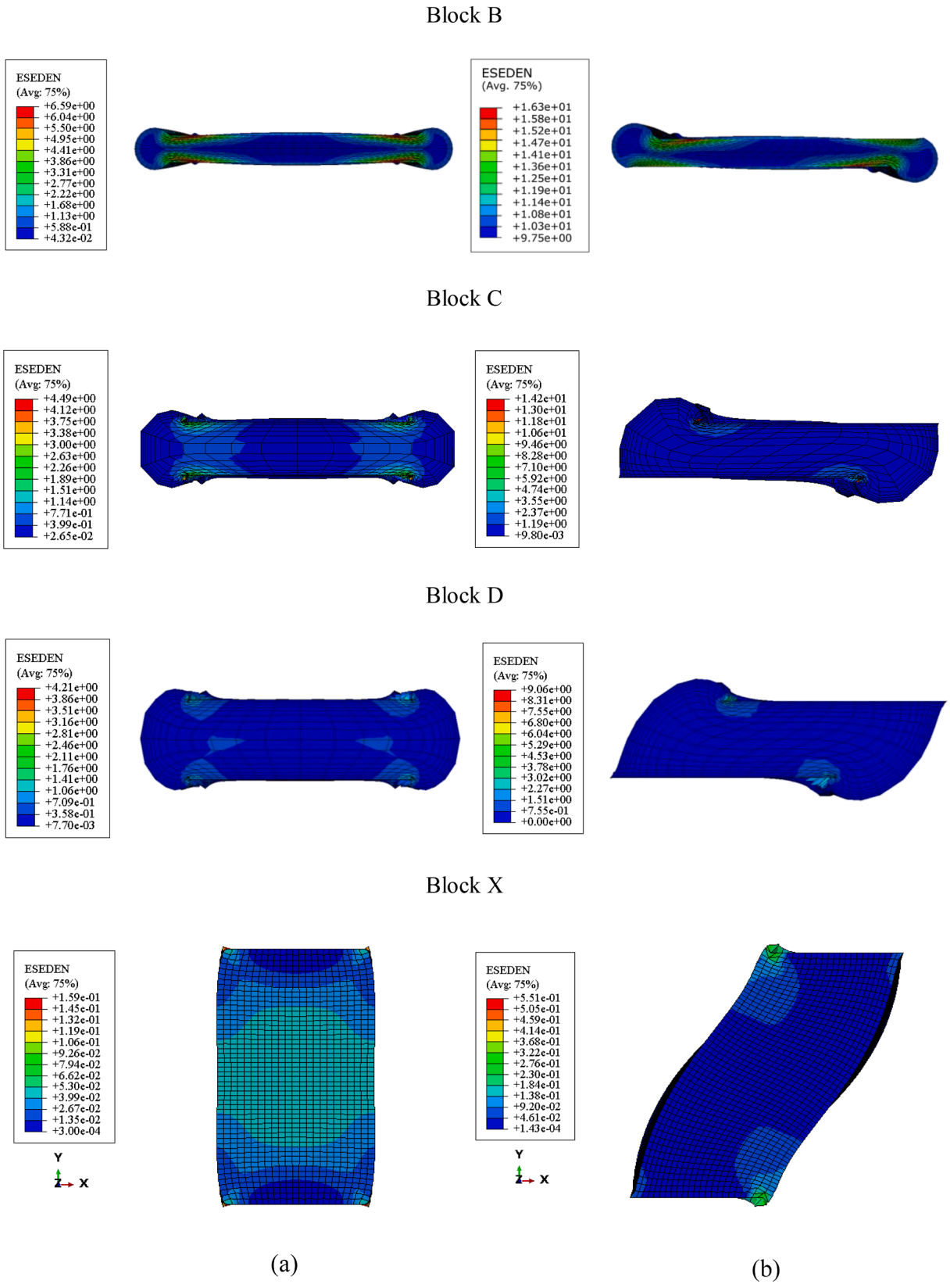

Fig. 7. Distribution of Total Strain Energy Density in N/mm^2 for half block subjected to (a) maximum compressive displacement alone and (b) maximum compressive displacement in combination with horizontal displacement.

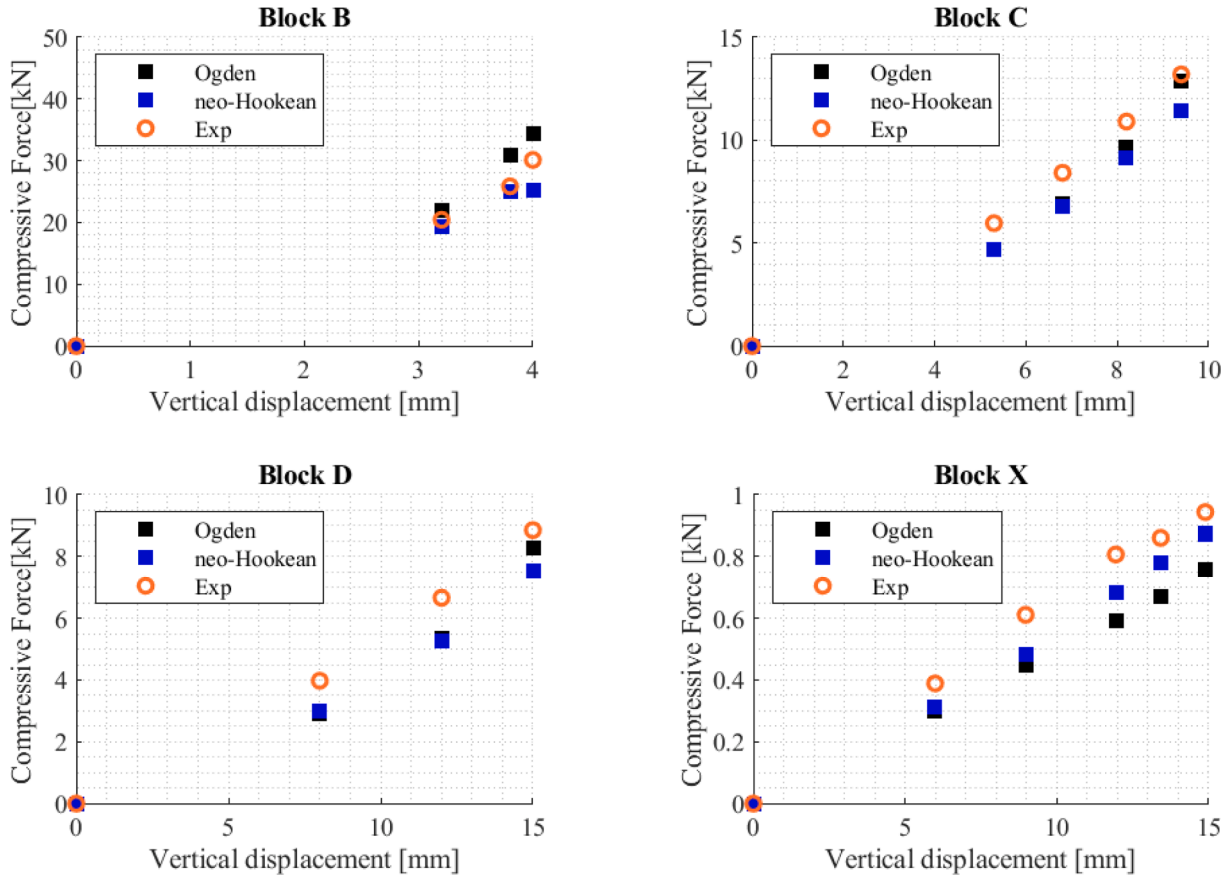

Fig. 8. FEA predictions of compressive load vs vertical displacement and comparison with experimental results.

$$\lambda^* = \frac{\lambda h_0 - \frac{1}{8}a_0}{h_0 - \frac{1}{8}a_0} \tag{6}$$

G is the shear modulus, A_0 is the initial cross-sectional area of the rubber block, and λ is the axial extension/compression ratio of the block, which is related to the strain through $\varepsilon = 1 - \lambda$. Since in this paper we are only discussing compression behaviour, we have chosen a sign convention such that the compression load P and deflection $\lambda(h_0\text{-}h)$ are both positive in compression, so that plots of load versus deflection appear in the positive quadrant. Indeed if the Haringx beam-column theory is used for both tensile and compressive behaviour, it is convenient to use two positive symbols for the load: P if it is compressive and N = -P if it is tensile, each expressible using real numbers in terms of trigonometric functions for P and hyperbolic functions for N (e.g. Goodchild et al, 2018).

Gent and Lindley (1959) carried out experimental tests on rubber blocks subjected to compression between rigid adhering plates and developed approximate load-deformation relations for circular disks and for infinitely long rectangular blocks. For the former case, they proposed the following expression of the effective compression modulus E_C

$$E_c = E\left(1 + 2kS^2\right) \tag{7}$$

where E is the Young's modulus of rubber, equal to $3G$ in the case of incompressible rubber, S is the shape factor, and $k \approx 1$ for unfilled rubber, but is an empirically determined factor less than unity used to take into account, albeit crudely, the strain-softening and imperfectly elastic stress–strain behaviour of filled rubber in simple shear. Lindley (1966) observed that Equation (7) also applies to rectangular blocks with comparable maximum and minimum plan dimensions, and is valid only under small strains.

Gent and Meinecke (1970) extended the theory of Gent and Lindley (1959) to the case of bonded rubber blocks of any cross-section under small compression. The vertical load P can be related linearly to the axial strain ε through the following expression:

$$P = A_0 E_c \varepsilon = 3GA_0(f_{c1} + f_{c2})(1 - \lambda) \tag{8}$$

where f_{c1} and f_{c2} are numerical factors describing the effect of the bonded surfaces. For a rectangular cross section with sides $2a$ and $2b$, these factors can be expressed as:

$$\begin{aligned} f_{c1} &= \frac{4}{3} - \frac{2\left(a_0 b_0 + h_0^2\right)}{3\left(a_0^2 + b_0^2 + 2h_0^2\right)} \\ f_{c2} &= \frac{4}{3}S_1^2(1+\kappa)^2\left[1 - \frac{192}{\pi^5}\kappa \sum_{n=1,3,5} \frac{1}{n^5}\tan\left(\frac{n\pi}{2\kappa}\right)\right] \end{aligned} \tag{9}$$

where $\kappa = a_0/b_0$.

For other sections, reference can be made to the original paper of Gent and Meinecke (1970).

The theories discussed above are derived by making three main assumptions: horizontal plane sections remain plane, vertical lines become parabolic after loading and the normal stress components in all three directions are the same, and equal to the mean pressure. Koh and Kelly (1989) proposed a solution of the compression modulus of bonded square rubber layers eliminating the stress assumption, whereas Tsai and Lee (1998) derived the compressive modulus of a bonded layer of infinite-strip, circular or square shape. Koh and Lim (2001) estimated the compressive modulus for the case of rectangular pads, providing an analytical solution as an extended version of the Koh and Kelly (1989) approach.

Kelly and Konstantinidis (2011) adapted the theories discussed above to the case of laminated bearings with values of shape factor $S >$

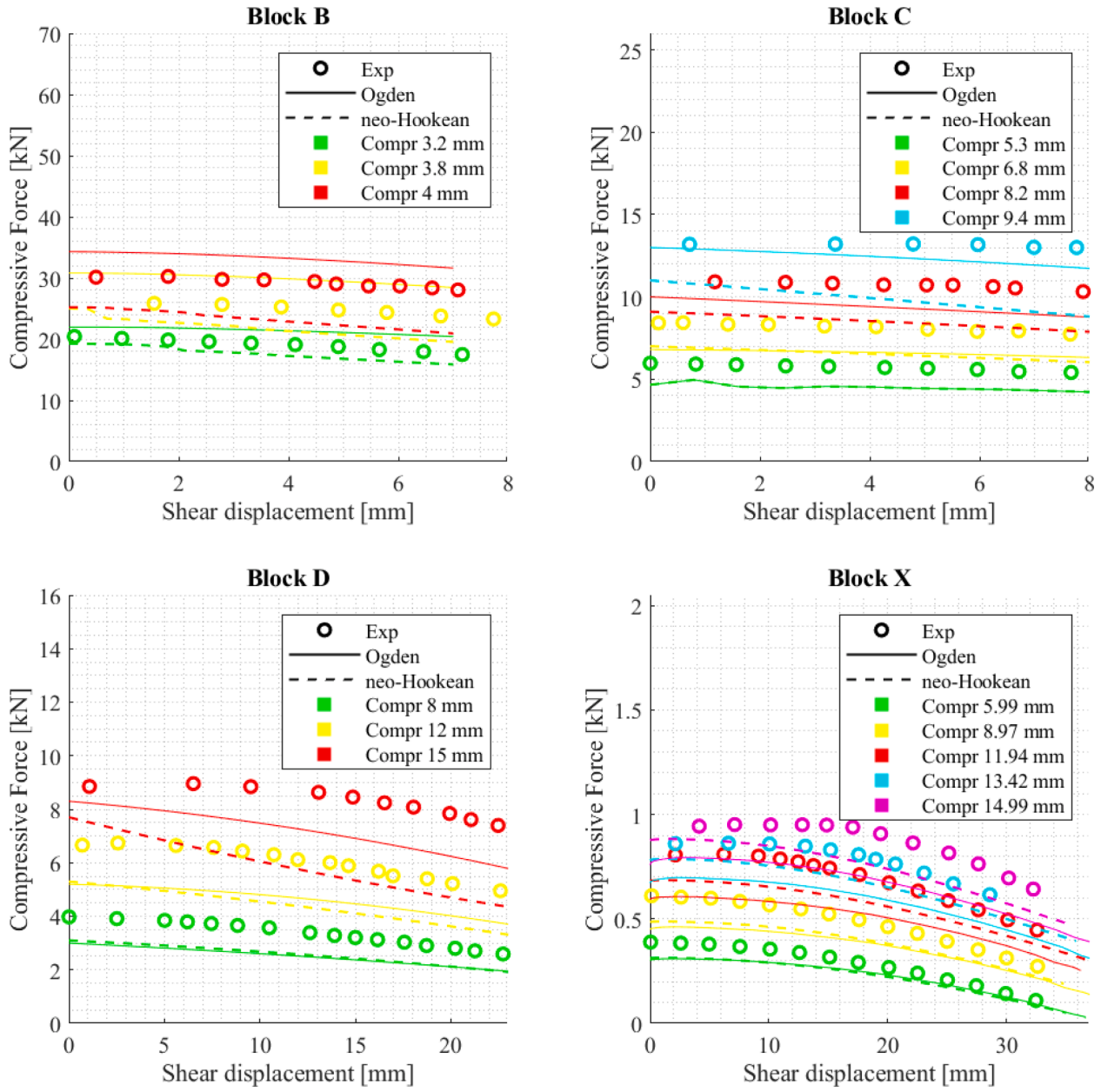

Fig. 9. FEA predictions of compressive force vs shear displacement of each block and comparison with experimental results (different colours refer to different values of the vertical compression).

5. They provided closed-form relations of the compression modulus for infinite strips and circular and rectangular pads. These expressions can be cast in the same form as Gent and Meinecke's expression (Equation (8)), with the numerical factor f_{c1} considered negligible and f_{c2} defined as in Equation (9).

Yeoh (1985) developed an expression for the compressive stiffness of tall cylinders of solid circular cross-section bonded at both ends to rigid plates, based on an improved description of the lateral constraining effect of the plates. However, he did not consider the case of rectangular blocks and assumed a linear behaviour and small strains.

Lindley (1966) provided an expression accounting for the non-linear relationship between force P and strain for a block of circular cross-section. He assumed the Young's modulus E to be independent of the state of strain and considered the increase of shape factor due to the decreasing thickness of the rubber block by a factor of $1/\lambda$, which coincides with the increase of loaded area of rubber:

$$P = 3GA_0\left[-\ln\lambda + S^2\left(\frac{1}{\lambda^2}-1\right)\right] \tag{10}$$

Equation (10) can be generalised to blocks of any cross-section by using the correction factors provided by Gent and Meinecke as follows (Cilento et al., 2017):

$$P = 3GA_0\left[-f_{c1}\ln\lambda + \left(\frac{1}{\lambda^2}-1\right)\frac{f_{c2}}{2}\right] \tag{11}$$

Goodchild et al. (2018) used the Mooney-Rivlin constitutive material, instead of a linear elastic one, to express the axial load–stretch relation for rubber strips (very slender rubber blocks) under a homogeneous strain field not perturbed by the end plates, corresponding to the following relationship:

$$P = 2A_0\left(\frac{1}{\lambda^2}-\lambda\right)\left(C_1+\frac{C_2}{\lambda}\right) \tag{12}$$

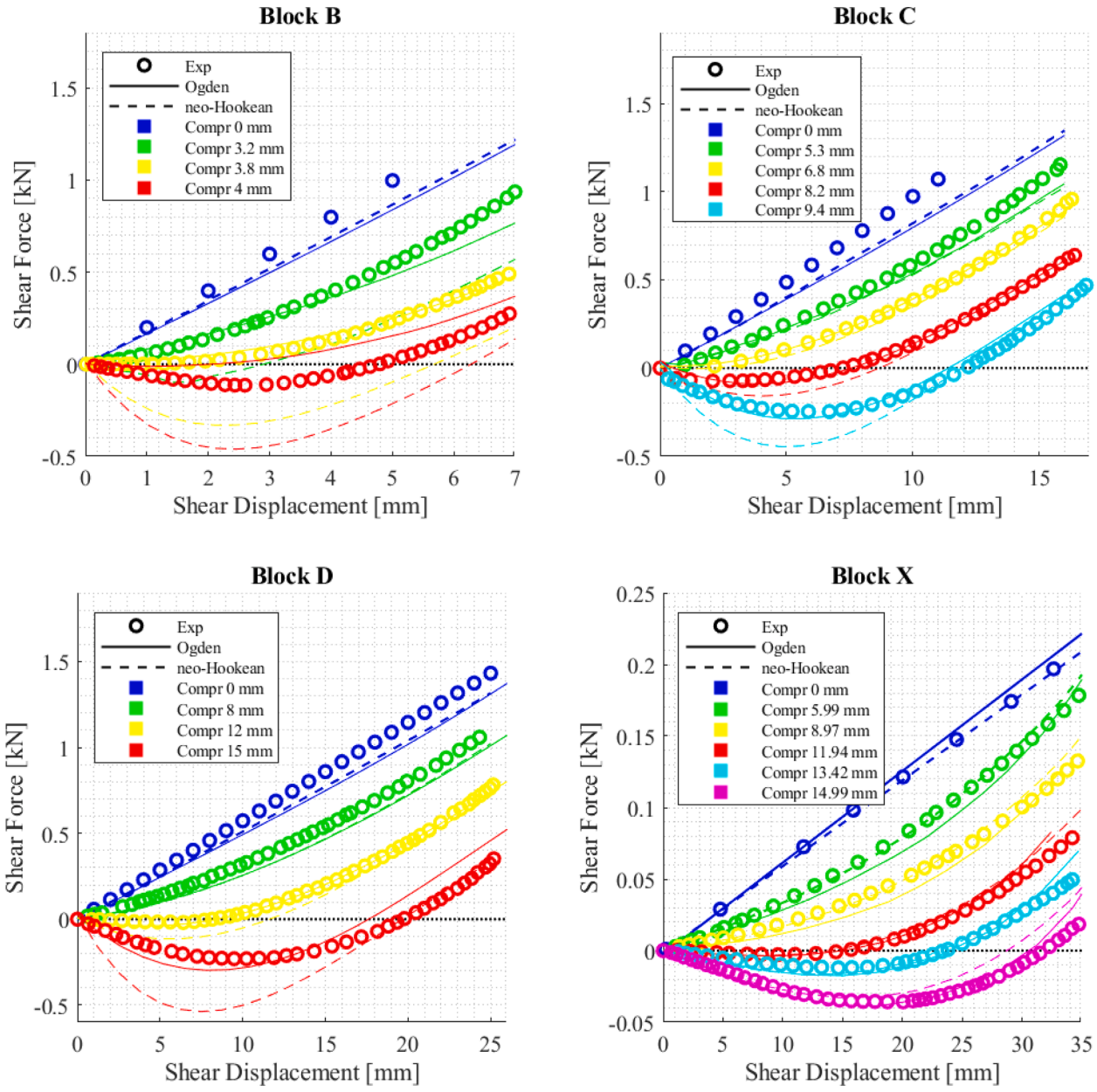

Fig. 10. FEA predictions of shear force vs shear displacement of each block and comparison with experimental results.

where C_1 and C_2 are material constants such that $G = 2(C_1 + C_2)$ for a Mooney-Rivlin material model (at zero shear deformation).

Muhr (2017) revised this formulation for application to the case of rubber blocks with bonded end-plates, obtaining the following expression, devised to reduce to Equation (10) for significant shape factors and to Equation (12) for a negligible shape factor:

$$P = GA_0\left[\left(\frac{1}{\lambda^2} - \lambda\right) + 3S^2\left(\frac{1}{\lambda^2} - 1\right)\right] \tag{13}$$

Stanton et al. (1990) also provided an extension of the classic theory of rubber blocks to include axial shortening and the increase in plan area due to bulging of an elastomer under compressive load. They consider a nominal Poisson ratio $\nu = 0.3$(rather than 0.5), chosen empirically to account for the non-uniform increase of area along the height due to the effect of the end plates. The theory assumes small deformation and a linear elastic material, and it was applied to the case of discreetly layered bearings. The model consists of a homogeneous shear flexible column, with compressive, shear and bending stiffnesses, which are functions of strain and are approximated by assuming that the plan dimension of each elastomeric layer increases by a factor $(1 + \nu(1\text{-}\lambda))$. The compressive force is:

$$P = 3GA_0(f_{c1} + f_{c2})\frac{(1+\nu(1-\lambda))^3 - 1}{3\nu(1-\lambda)}(1-\lambda) \tag{14}$$

In order to evaluate the accuracy of the different theories, the values of the axial load P are calculated using equations (5), (8), (11), (12), (13) and (14) for different values of the vertical deflection and compared with the experimental and numerical results in Fig. 12. The value of shear modulus G is 0.5 MPa.

The formula proposed by Gent and Meinecke (1970), reported here in Equation (8), valid for small compression levels, is not able to describe the nonlinear trend. Also the theory of Stanton et al., 1990, Equation (14), despite considering the increase of transverse area of the rubber due to Poisson's effect, significantly underestimates the compressive stiffness of the blocks. On the other hand, both the models of Lindley (1966), Equation (11), and Muhr (2017), Equation (13), agree well with

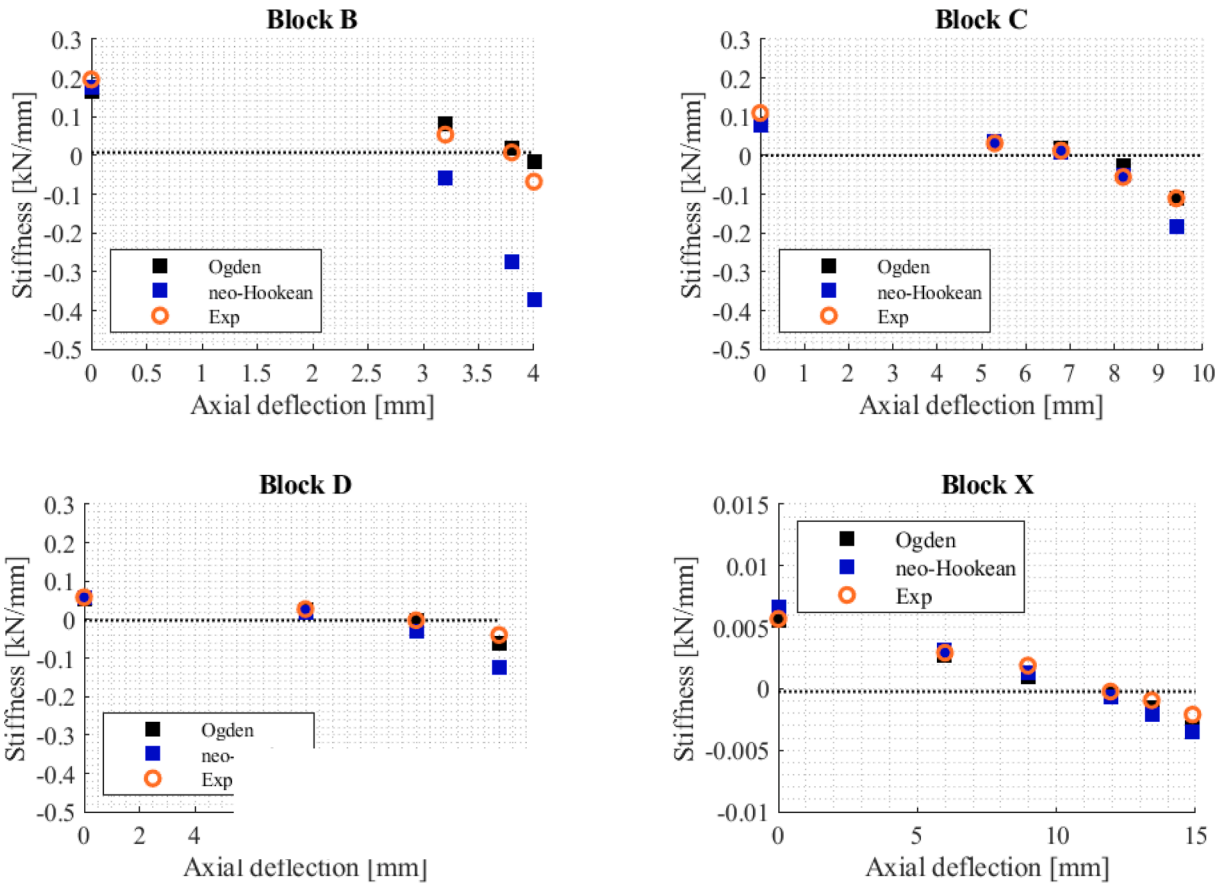

Fig. 11. Tangent horizontal stiffness (at zero shear deflection) vs. axial deflection: comparison between FEA and experimental results.

the experimental results.

In order to investigate further this issue, the secant compressive modulus $E_{c,\sec}$ at a given deformation level λ is evaluated considering the various formulations as follows:

$$E_{c,\sec} = \frac{P}{A_0(1-\lambda)} \tag{15}$$

The secant modulus is then normalized by dividing it by the value at zero deformation. Muhr (2017) derived the following expression for the normalized compressive secant modulus:

$$\frac{E_{c,\sec}}{E_{c0}} = \frac{\frac{1}{\lambda^2}\left\{\left(\lambda^2+\lambda+1\right)+3S^2(\lambda+1)\right\}}{3\left(1+2S^2\right)} \tag{16}$$

where E_{c0} coincides with $E_{c,\sec}$ for $\lambda = 1$. In the case of $S = 0$ (homogeneous strain field not perturbed by the plates), this relation reduces to the one found by Goodchild et al. (2018).

The normalized secant compression modulus from Stanton's theory has the following expression:

$$\frac{E_{c,\sec}}{E_{c0}} = \left(1+\nu(1-\lambda)+\frac{\nu^2(1-\lambda)^2}{3}\right) \tag{17}$$

Fig. 13 shows the variation with λ of the secant compression modulus defined by the above equations and by the FEA results obtained by using the neo-Hookean material model.

In general, the FE analyses reveal a high sensitivity of the ratio $E_{c,\sec}/E_{C0}$ with respect to λ and also with respect to the shape factor S. It can be observed that the ratio $E_{c,\sec}/E_{C0}$ increases for decreasing λ and increases for increasing shape factor. The secant compression modulus according to Stanton et al.'s model is not very sensitive to λ, and independent of the shape factor. Muhr's theory is capable of accounting for the dependency of the secant compressive modulus on both the axial shortening and the shape factor, although there are discrepancies with the FEA results.

4.2. Combined compression and shear behaviour

The theory for the behaviour of flexural-shear deformable elastic beams under the combined action of compressive and shear forces was originally developed by Timoshenko (1921). Haringx (1948, 1949a, 1949b), derived a similar theory for application to coil springs and rubber cylinders, and Gent adapted this for application to rubber laminated bearings (Gent, 1964). The model at the base of these theories is a flexural-shear deformable column of length h_0 subjected to an axial compressive load P; in this paper we shall assume that the axial direction is vertical and the lateral direction is horizontal. The kinematics can be described by the lateral displacement of the centre line $v(x)$, and the rotation of the cross section, $\psi(x)$. A horizontal force F is applied at the upper end which is free to move horizontally but is restrained from cross section rotation, while the lower end of the column is fixed. In the linear elastic case, the following expression of the horizontal stiffness of the beam is obtained (Thomas, 1982):

$$K_h = \frac{P^2}{Ph - 2qB\tan\left(\frac{qh}{2}\right)} \tag{18}$$

where

$$q^2 = \frac{P(R-P)}{BR} \tag{19}$$

In equation (19), B and R are the bending and shear stiffness parameters for unit length of the column, respectively, derivable from constitutive relations for the particular type of beam-column in mind.

From equation (18), the lateral stiffness of the block would fall to

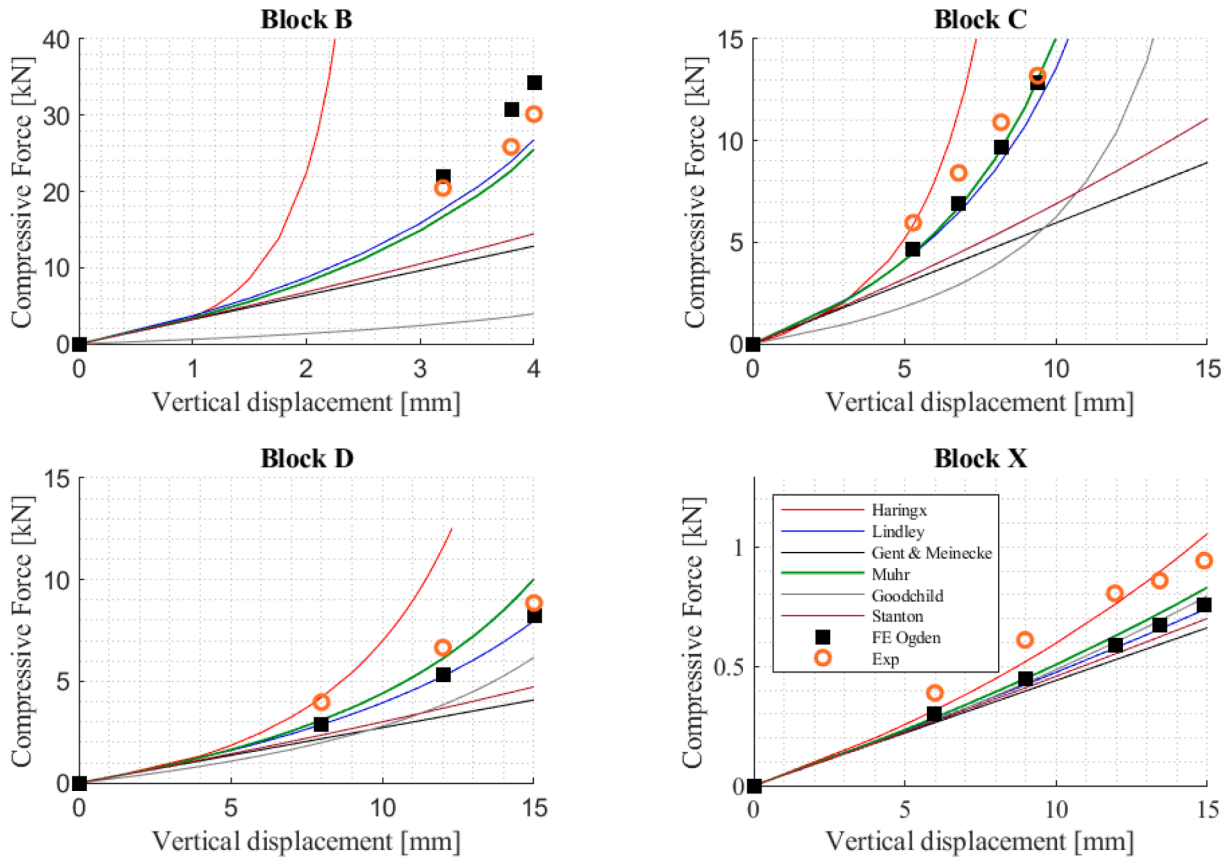

Fig. 12. Force-displacement behaviour according to equation (5) (Haringx's theory) equation (8) (Gent and Meinecke's theory), equation (11) (Lindley's theory), equation (12) (Goodchild's theory), equation (13) (Muhr's theory) and equation (14) (Stanton's theory) and experiments. FE results (Ogden) from Fig. 8 are also reported.

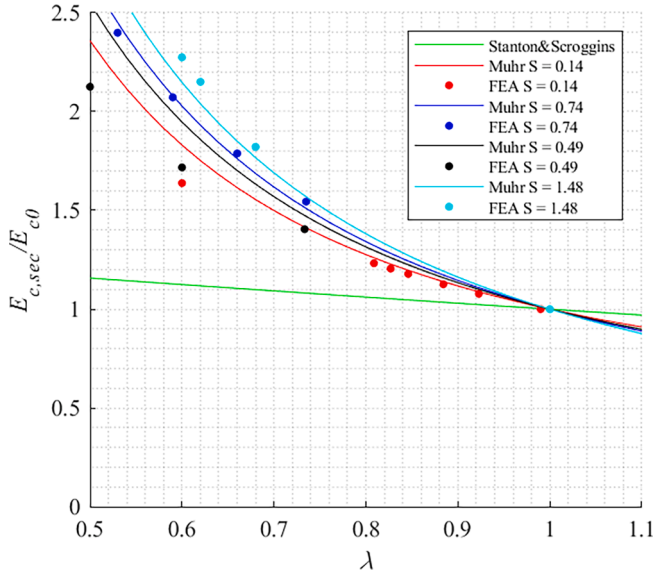

Fig. 13. Effect of vertical compression on secant compression modulus.

zero if $(q/2)h \to \pi$. Under this condition, the term $\tan((q/2)h/2) \to \infty$ and the compressive load P attains a critical value P_{cr}, given by

$$\frac{P_{cr}}{B}\left(1+\frac{P_{cr}}{R}\right)=\frac{\pi^2}{h^2} \tag{20}$$

This equation can be solved for P_{cr}, to obtain the expression of the critical load:

$$P_{cr}=\frac{R}{2}\left[-1+\sqrt{1+\frac{4\pi^2 B}{Rh^2}}\right] \tag{21}$$

Thomas et al. (1982) assumed B, R and h in the undeformed initial configuration. Bending and shear stiffness parameters have been derived by Haringx for the case of a rubber rod in (Haringx, 1949b). Gent (1964) provided these parameters for the case of laminated rubber bearings, further refined by Gent and Meinecke (1970) and extended to any cross-section. Goodchild et al. (2018) derived expressions for the bending and shear stiffness of a rubber prism, modelled as a Mooney material, as functions of finite-strain axial elongation. Muhr (2017) investigated the applicability of the expressions of Goodchild et al. (2018) to blocks of rubber with bonded end faces. The bending stiffness $B = E_{C,bend}I$ corresponding to an axial elongation λ was obtained from an incremental Young's modulus, $E_{C,bend}$, referred to the strained state and expressed as a function of the shape factor, and the second moment of area of the cross section in the deformed state, I. The expression obtained for $E_{C,bend}$ is:

$$E_{C,bend} \approx G\left(2\lambda^2+\frac{1}{\lambda}\right)\left(1+\frac{2S^2}{3}\right) \tag{22}$$

This reduces to the case of Goodchild et al. (2018) for $S = 0$.

The expression of I for a deformed rectangular rubber prism normal to its axis was taken to be:

$$I=\frac{a^3 b}{12}=\frac{a_0^3 b_0}{12\lambda^2}=\frac{I_0}{\lambda^2} \tag{23}$$

where I_0 is the second moment of area of the cross section in the

undeformed state.

The shear stiffness parameter according to Goodchild et al. and Muhr's theory is evaluated as follows:

$$R = \frac{A_0}{\lambda}\frac{\tau_{12}}{\gamma} = \frac{A_0}{\lambda}\frac{1}{\gamma}\left[2\gamma\lambda^2\left(\frac{\delta U}{\delta I_1} + \frac{1}{\lambda}\frac{\delta U}{\delta I_2}\right)\right] = 2A_0\lambda\left[C_1 + \frac{1}{\lambda}C_2\right] \tag{24}$$

For $C_2 = 0$, as assumed by Muhr (2017) and throughout the remainder of this paper:

$$R = \lambda G A_0 \tag{25}$$

Stanton et al. (1990) suggested an expression of the bending stiffness, intended for rubber bearings with multiple laminations rather than a single block, in the form:

$$B = f_r E I_0 (1 + \nu^*(1-\lambda))^4 \tag{26}$$

where ν^* is a fitting parameter akin to Poisson's ratio, but of uncertain magnitude, and f_r is the bending stiffness factor (Gent and Meinecke, 1970), taken here as $f_r = 1 + 0.5S^2$.

The shear stiffness parameter according to Stanton's theory is:

$$R = G A_0 (1 + \nu^*(1-\lambda))^2 \tag{27}$$

The global lateral stiffness K_h from Muhr's theory is obtained by substituting Equations (22), (23) and (24) into Equation (18) and considering the rubber height in the deformed configuration, evaluated as $h = \lambda h_0$, reducing to Goodchild's expression if the shape factor is zero; Stanton's theory is applied by substituting (26) and (27) into (18).

It is noteworthy that in a conventional Euler column, the reduction in transverse stiffness caused by axial load can be approximated by:

$$K_h = K_{h0}\left(1 - \frac{P}{P_{cr}}\right) \tag{28}$$

where K_{h0} denotes the horizontal stiffness for zero compression.

In the case of a shear-flexible column such as the one considered in Haringx's theory, under some simplifying assumptions, the following expression can be derived, as also discussed in Roeder et al. (1987):

$$K_h = K_{h0}\left(1 - \left(\frac{P}{P_{cr}}\right)^2\right) \tag{29}$$

Fig. 14 compares the plots of the horizontal stiffness vs. the axial deflection according to these theories and the experimental results. Shown in the same figure are the plots corresponding to Equation (29) and to Haringx's theory, i.e. Equation (18) with the bending and shear stiffness parameters defined in (Haringx, 1949b) for rubber rods, with his end "correction" to allow for the lateral restraint of bonding the rubber to rigid endplates. Goodchild et al.'s theory is appropriate only for the lowest shape factor considered ($S = 0.14$), whereas for higher shape factors it provides horizontal stiffness values almost constant as the axial deflection increases. This demonstrates the high importance of the shape factor on the compressive modulus of the rubber in evaluating the behaviour of the rubber blocks. Stanton's theory, instead, captures the trend of decrease of the horizontal stiffness due to the axial deflection. Muhr's theory provides quite good estimates of the horizontal stiffness for Block X and is also able to describe the effect of the compression with quite good accuracy. However, shear stiffness predictions for the other blocks diverge from the experimental results to a progressively greater extent as the compression is increased, and the model fails to predict the observed instabilities at the highest compressions. The next section presents a modified theory to meet these shortcomings.

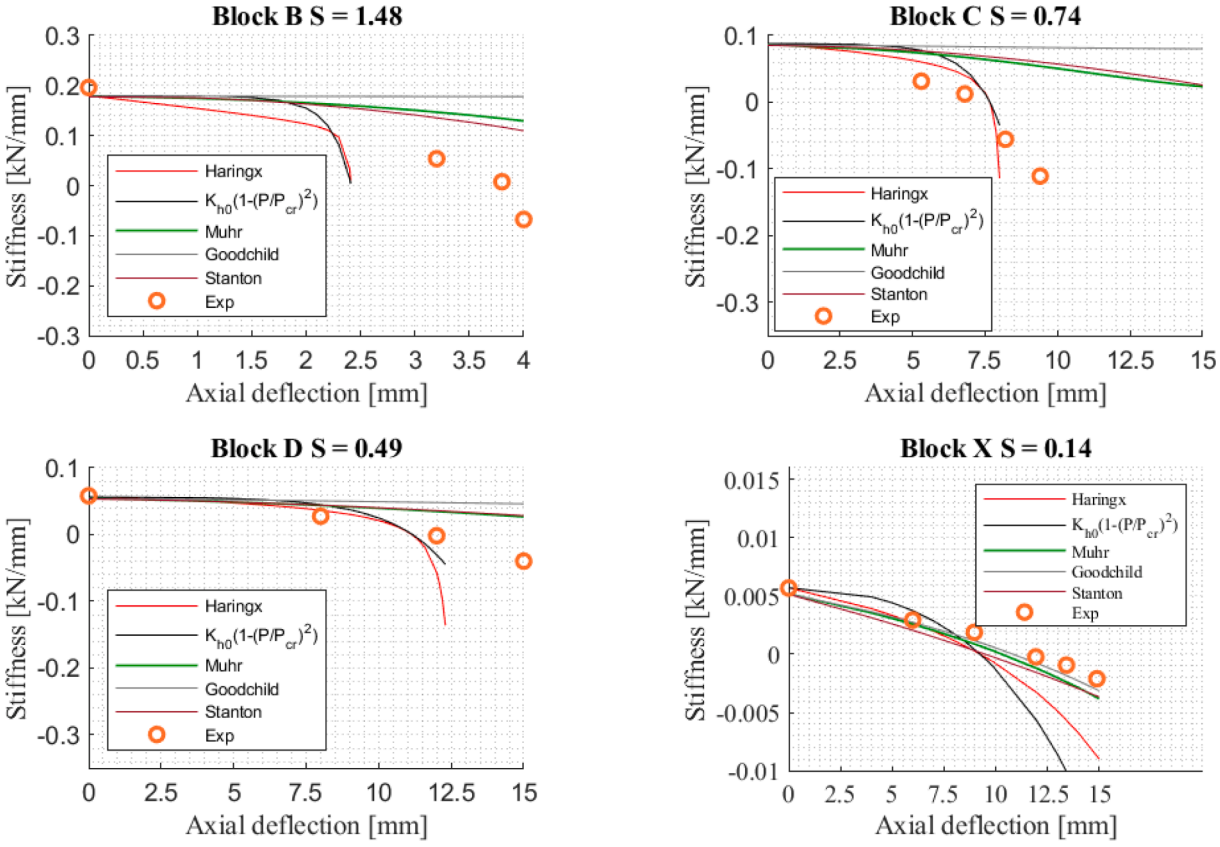

Fig. 14. Tangent horizontal stiffness (at zero shear deflection) vs axial deflection: comparison between experimental tests and analytical estimates obtained according to equation (18), with B and R evaluated using Haringx, Muhr, Goodchild and Stanton theories, and equation (29).

4.3. Improved theory for lateral stiffness of compressed rubber blocks

For low and moderate shape factors rubber may be assumed to be incompressible, so that when a rubber block is compressed, each side bulges laterally such that the volume is kept constant. Fig. 15 shows an example of a square block (W_0 is the initial width of the transverse section) made of an incompressible rubber, which is compressed in the vertical direction by λ. Since the volume is constant, the deformation on the two horizontal directions is $1/\sqrt{\lambda}$. This is true only in the case of an unconfined rubber block (Fig. 15a). On the other hand, in the case of a rubber block bonded at each end, the stretch along the horizontal directions is higher than $1/\sqrt{\lambda}$ (Fig. 15b) in the middle section, and decreases towards unity at the bond edge.

The theory of Stanton et al. (1990) accounts for the bulging in a simplified way by introducing an "equivalent Poisson ratio" ν^* which they chose to be 0.3; if the block is compressed by a strain of $\varepsilon = 1\text{-}\lambda$, it will bulge and increase laterally its dimensions by, on average, the factor $\nu^*\varepsilon$ so that the cross sectional area will become $A \approx (1+\nu^*\varepsilon)^2 A_0$ and the second moment of area will become $I \approx (1+\nu^*\varepsilon)^4 I_0$.

FE analyses, using the neoHookean material model, have been performed to investigate further the effect of the non-uniform bulging on the shear and tilting stiffness. For this purpose, Block B (Fig. 16) is considered. This is a very stocky block, for which the response to horizontal deflections is dominated by shear deformation. Subjecting an FE model of Block B to a shear loading without applying any pre-compression results in a horizontal stiffness of 174 kN/m, close to the value of 180 kN/m evaluated for a block under simple shear, GA_0/h_0, where A_0 is cross-sectional area. Another block is considered (Fig. 17a), with dimensions that correspond to the reduced height and an idealised bulged area of block B of incompressible rubber subjected to the maximum compression load observed experimentally (30kN). The plate dimensions are the same as in the original block, i.e., the extended portion of the block is not confined. When this block is subjected to a shear loading (Fig. 17b), the unconfined parts of the block tilt without deforming, and thus they do not contribute to the shear stiffness. The shear stiffness evaluated numerically, equal to 270 kN/m, is comparable to that obtained with the simple expression $GA_0/h = 300$ kN/m, considering A_0 as shear area and h as height 6 mm. Therefore, it can be concluded that under horizontal deflections, only the rubber within the area of the reinforcing plates contributes to the shear behaviour. This effect is also evident in shear of pre-compressed blocks, as shown in Fig. 6b.

In the original theory of Goodchild (2018), R was taken to be equal to $\frac{A_0}{\lambda}\frac{\tau_{12}}{\gamma}$ (see the Appendix of Goodchild et al. (2018) and Equation (24) above), which neglects the absence of tractions on the lateral free surface of the rubber, and thus the effect shown in Fig. 17b and evident also in Fig. 6b. This observation suggests the shear parameter would be reduced by approximately the factor $A_0/A = \lambda$ leading to a revision to the value of R by the same factor, which yields

$$R = GA_0\lambda^2 \tag{30}$$

Equation (30) gives a stronger softening effect on the shear parameter at a given compression than in Muhr's theory (Equation (25)).

On the other hand, the bulging is expected to contribute to the bending stiffness of the rubber blocks. This contribution is found to be evident for more slender blocks such as Block X, for which the effect of the confinement of the plates is small, whereas it is expected to be negligible for stocky blocks such as block B, for which the behaviour is dominated by shear compliance.

A novel expression is proposed for the second moment of area I to be considered in evaluating the tilting stiffness. Instead of using Equation (23), this is expressed as $I = I_0\Psi^2$, where Ψ is a correction factor describing the effect of the confinement of the plates on the rubber block bulging. The aspect ratio a_0/h_0 (a_0 being in direction of shear loading) is used to define the effect of the bulging. It is noteworthy that in the case of incompressible rubber ($E = 3G$), this factor is equal to:

$$\frac{a_0}{h_0} = 4\sqrt{\frac{EI_0}{h_0^2 GA_0}} \tag{31}$$

Thus, this geometrical parameter is related to the shear parameter of Timoshenko theory defined as $\Omega = EI_0/GA_0h_0^2$ (Wang, 1995) which describes the relative importance of shear compliance over the bending compliance. In fact, GA_0/h_0 is the shear stiffness and EI_0/h_0^3 is the flexural stiffness. When EI_0/h_0^3 is small, i.e. small a_0/h_0, there is a higher contribution of flexure, whereas when GA_0/h_0 is small, i.e. high S_2, there is a higher contribution of shear deformability. In the case of laminated rubber bearings, the ratio between the rubber layer width and total bearing height is denoted as secondary shape factor (Montuori et al., 2016).

The following semi-empirical expression for Ψ was devised to give the best fit to the FE analysis results:

$$\psi = \begin{cases} \left(\dfrac{1}{0.125a_0/h_0 + \sqrt{\lambda}\left(1 - 0.125(a_0/h_0)^2\right)}\right)^2 & (a_0/h_0)^2 < 8 \\ 1 & (a_0/h_0)^2 \geqslant 8 \end{cases} \tag{32}$$

It can be noted that $\Psi = 1/\lambda$ for $(a_0/h_0)^2 = 0$, as in Muhr's original theory, since the effect of the confinement is not significant in an infinitely slender block, whereas $\Psi = 1$ for $(a_0/h_0)^2 \geq 8$, since in stocky blocks the confinement is very significant.

The value of the bending stiffness parameter, which has been modified using Ψ to take into account the bulging effect, is

$$B = E_{C,bend} I_0 \psi^2 \tag{33}$$

Fig. 18 shows the results obtained using the expression of the shear stiffness of equation (30) and of the bending stiffness of equation (33) with $E_{C,bend}$ defined from equation (22). It also shows the comparison with Muhr theory, experimental and numerical results. It can be observed that the modified theory provides an excellent fit to the results, both FEA modelling and experimental.

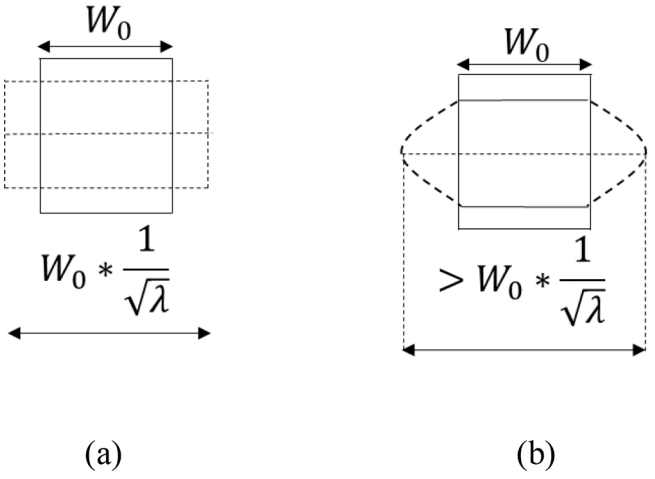

Fig. 15. Incompressible rubber block subjected to a vertical compression: (a) unbonded rubber block, (b) bonded rubber block.

4.4. Critical load

Table 3 shows the predicted critical loads from the Haringx theory, equation (21); Stanton et al. model, equation (21) with bending and shear stiffness expressed as functions of their Poisson ratio parameter and adapted to the case of rubber blocks; extended theory, equation (21), with bending and shear stiffness evaluated with equations (33) and (30), and h is the rubber block height in the deformed configuration due

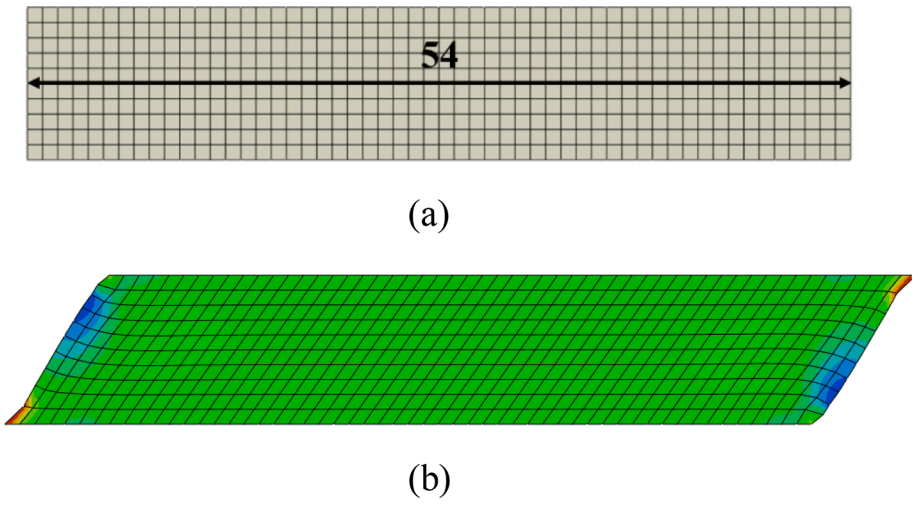

Fig. 16. Block B (a) Undeformed configuration (b) Deformed configuration due to the highest shear load observed experimentally. Modified geometry to simulate the behaviour with the additional area.

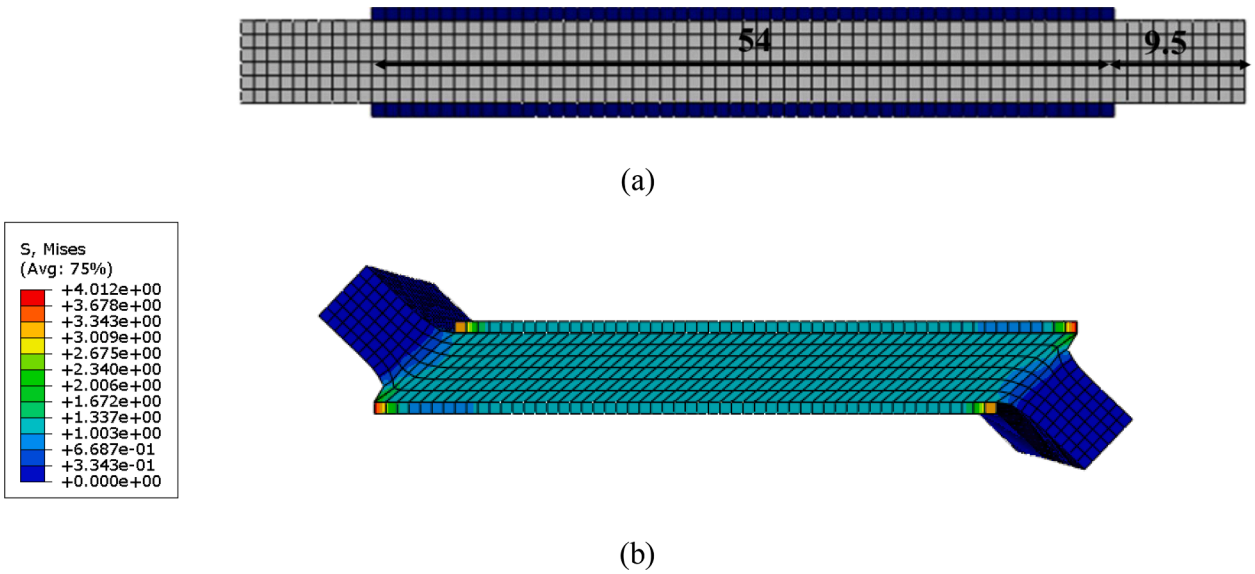

Fig. 17. Block B, modified geometry to simulate the shear behaviour of the block of Fig. 16 when precompressed (a) Unsheared configuration (b) Sheared configuration due to the highest shear load observed experimentally.

to the compressive load. Table 3 also reports the values of the critical load according to Lanzo's theory. Lanzo (2004) provided a closed form of the critical load of multi-layered rubber bearings on the basis of a linear elastic model, derived from the classical beam theory, but enriched with the axial deformability in addition to the shear and flexural deformability, as follows:

$$P_{cr} = \frac{-1 + \sqrt{1 + \frac{4\pi^2 B}{h_0^2}\left(\frac{1}{R} - \frac{1}{EA}\right)}}{2\left(\frac{1}{R} - \frac{1}{EA}\right)} \tag{34}$$

However, similarly to Haringx's theory, this theory does not account for the dependency of bending and shear stiffnesses on axial shortening and shape factor.

These values are compared against the critical load obtained from experimental and numerical results by means of an average percent error defined as follow:

$$\Delta\% = \frac{\sum_{i=A,B,C,D} |\Delta\%_i|}{4} \tag{35}$$

Where $\Delta\%_i$ denotes the percentage difference between the analytical estimates and the experimental or numerical estimate for block i, with i = A,B,C,D.

It is remarkable that the estimates of P_{cr} calculated naively from the Stanton or Lanzo theories are not wildly different from the FEA or Experimental results, since these theories are based on a continuum beam-column limit for bearings comprising a sufficiently large number of identical layers laminated in series such that the discreteness of the layers may be smeared into a continuum (see Schapery and Skala, 1976; Gent, 1964). It can be observed that Haringx's theory overestimates the critical load when compared to both numerical and experimental results for Block B, C and D, whereas for Block X the value is underestimated. Stanton et al.'s theory overestimates the critical load when compared with experimental results, for Block C and D. Lanzo's theory provides higher critical loads with respect to the Gent theory due to contribution of the axial deformability of the rubber block, but it gives the highest average percent error when compared to the numerical results. The extended theory, which attempts to include effects of non-linearity and finite strain, provides overall the best estimates when compared to the

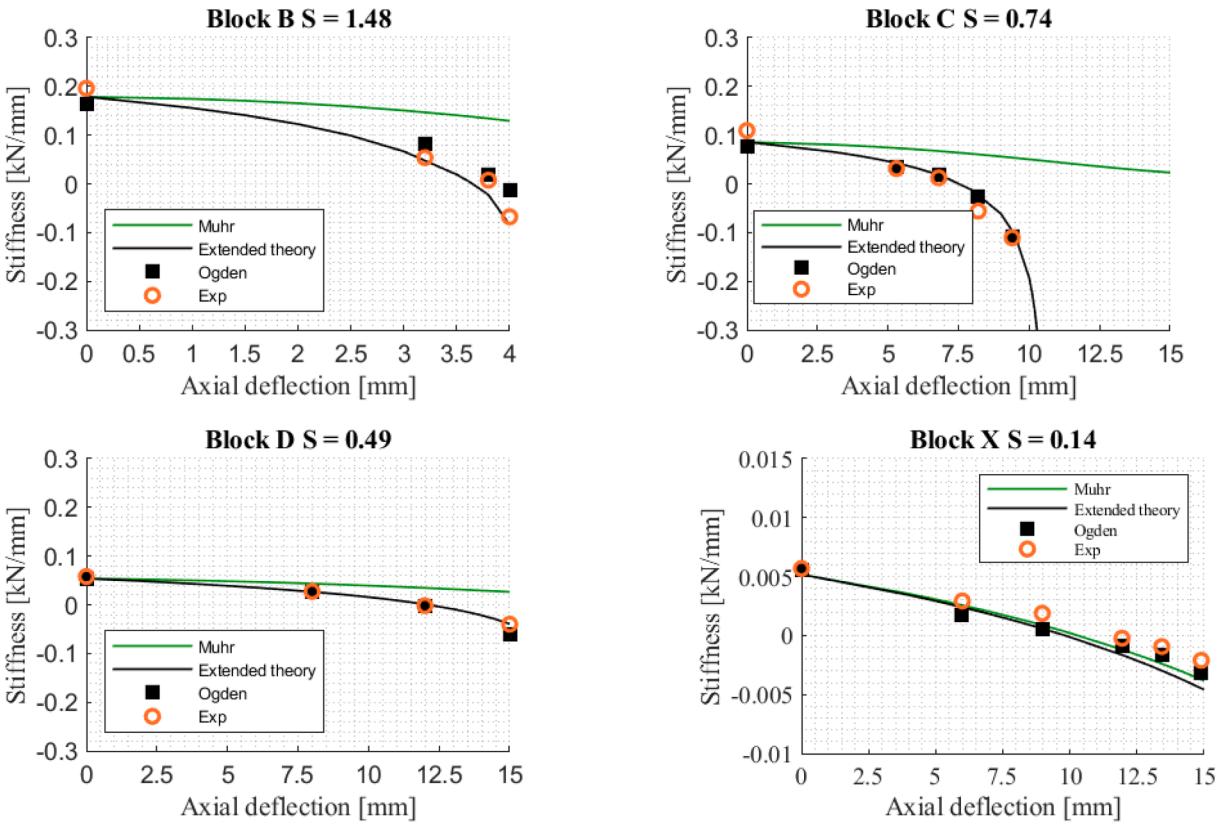

Fig. 18. Tangent horizontal stiffness (at zero shear deflection) vs axial deflection: comparison between experimental tests and analytical results obtained with Muhr and the proposed extended theory.

Table 3
Predicted and experimental critical loads and average percent errors.

	Haringx	Stanton et al. (1990)	Lanzo (2004)	Extended theory	FEA Ogden	FEA neo-Hookean	Experim.
	P_{cr} (kN)	P_{cr} (kN)	P_{cr} (kN)	P_{cr}(kN)	P_{cr} (kN)	P_{cr} (kN)	P_{cr} (kN)
Block B	60.4	24.5	17.4	21.0	30.8	25.0	26.0
Block C	17.0	14.0	10.1	8.2	6.9	6.8	8.4
Block D	9.2	8.1	6.3	6.3	5.3	5.3	6.7
Block X	0.50	0.44	0.41	0.50	0.59	0.68	0.81
Δ%to Experim.	70%	35%	27%	17%	21%	15%	0%
Δ%to FEA (Ogden)	80%	25%	34.4%	24.4%	0%	9.5%	24.6%
Δ%to FEA (neo-Hookean)	90%	50%	34.8%	20.7%	10%	0%	18.4%

numerical results. Finally, it can be observed that both Ogden and neo-Hookean material models are in good agreement with experiments. It is noteworthy that the Ogden material model provides higher values of the critical load for all blocks expect for Block X. This is consistent with the results shown in Fig. 9 where it can be observed that the Ogden model is stiffer for the same blocks, presumably because the Ogden model is softer than neo-Hookean only in homogeneous compression (Fig. 4), which is the predominant mode of deformation only for Block X.

5. Conclusions

The behaviour of bonded rectangular blocks with low shape factor subjected to vertical and horizontal loading is investigated in this study by a combination of experimental, numerical, and theoretical studies. When compressed, these blocks are characterised by significant shortening and bulging, two effects that significantly influence their mechanical behaviour under shear loading.

Based on the results of the experimental and numerical investigations, the following conclusions can be drawn:

- The investigated blocks behave very differently under the applied horizontal deflection, with the block of highest shape factor deforming mainly in shear, and the lowest shape factor block deforming mainly under bending.
- The Ogden material model provides more accurate results than the neo-Hookean model, particularly for high vertical compressions.
- The analysis of the local distribution shows high concentration of stresses in the case of the stocky block. The analyses also reveal the formation of a compression strut under shear deflection of a compressed block, and the concentration of tensile stresses and strain at top right and bottom left areas of the blocks when the top is displaced to the right. These could be important for defining limit conditions in the blocks, e.g. related to cavitation or delamination.
- When compressed blocks are sheared, only very modest shear strains are generated in the rubber that has bulged beyond the reinforcing plates

The second part of the paper investigates the applicability of alternative theories for describing the compressive behaviour first and then the combined compressive and shear behaviour of slender rubber blocks. With regards to the compressive behaviour, it is observed that Muhr and Lindley's theories, which include the influence of the axial shortening and shape factor on compressive load, are found to provide very good approximations of the load–displacement response and of the secant compression modulus. With regard to the description of the horizontal stiffness of the blocks under constant vertical compression, it is concluded that:

- According to Haringx's theory, the horizontal stiffness decreases very rapidly with the increase of vertical compression, with critical values obtained for small axial compression levels.
- Stanton's theory, accounting for the height reduction and increase of plan area due to compression, but within the hypotheses of small deformations and a linear elastic material, provides more accurate results than Haringx's theory, but they are still quite far from the experimental and FE simulations;
- The theory of Muhr, accounting for the height reduction and increase of plan area due to compression with a finite deformation formulation, but disregarding the non-uniform bulging of the compressed blocks, provides good estimates of the horizontal stiffness only for small compressions, or, at large compression, for the case of very slender blocks.
- The proposed extended theory, which starts from the theory of Muhr but provides an improved description of the non-uniform bulging of the compressed blocks on the shear and bending stiffness, is able to accurately describe the horizontal stiffness variation with the axial deflection for all the blocks considered.
- In the final part of the paper, the estimates of the critical load according to the numerical and various theoretical models are computed and compared with the experimental ones. Also in this case, the proposed theory yields the best prediction of the critical load and outperforms the other theories when compared to the experimental and FE results.
- It is remarkable that the theories that include the shape factor effect of bonded end plates (Lanzo, Stanton et al., Muhr and the Extended theory) work so well for a single block despite the non-uniform lateral restraint (due to bonded endplates) along the length of the block, and the treatment of it as being a beam column with a uniform constitutive behaviour along its axis. This observation implies that the theories are expected to have similar accuracy, or better, for beam columns consisting of several such units in series.

Declaration of Competing Interest

The authors declare that they have no known competing financial interests or personal relationships that could have appeared to influence the work reported in this paper.

Data availability

Data will be made available on request.

References

'Dassault Systèmes, Abaqus Analysis User's Manual Version' (2018).

Aiken, I.D., Kelly, J.M., Tajirian, F.F., 1989. Mechanics of Low Shape Factor Elastomeric Seismic Isolation Bearing. University of California, Berkeley. Report No. UCB/EERC-89/13,.

Cardone, D., Perrone, G., 2012. Critical load of slender elastomeric seismic isolators: an experimental perspective. Eng. Struct. 40, 198–204. https://doi.org/10.1016/j.engstruct.2012.02.031.

Chalhoub, M.S., Kelly, J.M., 1990. Effect of bulk compressibility on the stiffness of cylindrical base isolation bearings. Int J. Solids Structures 26 (7), 743–760.

Cilento, F., Vitale, R., Spizzuoco, M., Serino, G., Muhr, A.H., 2017. Dynamic behaviour in compression and shear of low shape factor rubber blocks. Atti del XVII Convegno ANIDIS L'Ingegneria Sismica in Italia: Pistoia 36 (2), 86–102.

Fan, L. J., Muhr, A. H., Parsons, B. and Thomas, A. G. (1992). Shear load-deflaction behaviour of compressed Rubber blocks. Rubbercon 92, Brighton. TARRC Reprint 1420.

Gent, A.N., 1964. Elastic Stability of Rubber Compression Springs. Rubber Chem. Technol. 6 (4), 318–326. https://doi.org/10.1243/JMES_JOUR_1964_006_046_02.

Gent, A. N. and Lindley, P. B. (1959). The Compression of bonded rubber blocks. Rubber Chem. Technol., 173(1), pp. 111–122. https://doi.org/10.1243%2FPIME_PROC_1959_173_022_02.

Gent, A.N., Meinecke, E.A., 1970. Compression, bending, and shear of bonded rubber blocks. Polym. Eng. Sci. 10, 48–53. https://doi.org/10.1002/pen.760100110.

Goodchild, I.R., Muhr, A.H., Thomas, A.G., 2018. The lateral stiffness and damping of a stretched rubber beam. Plast., Rubber Compos. 47 (4), 176–186. https://doi.org/10.1080/14658011.2018.1459065.

Gough J, Muhr AH. Initiation of failure of rubber close to bondlines. Proc. International Rubber Conference. 2005, Maastricht. IOM Communications Ltd, London, 165-174.

Haringx, J.A., 1948. On highly compressible helical springs and rubber rods, and their application for vibration-free mountings, I. Philips Res. Rep. 3, 401.

Haringx J. A., (1949)a. On highly compressible helical springs and rubber rods, and their application for vibration-free mountings, II, Philips Res. Rep.**4** 49.

Haringx J. A., (1949)b. On highly compressible helical springs and rubber rods, and their application for vibration-free mountings, III, Philips Res. Rep.**4** 206.

Haringx, J. A. (1949)c. Elastic stability of helical springs at a compression larger than original length. Applied Sciences Research. 1, pp. 417–434. https://doi.org/10.1007/BF02120345.

Hirst, A. J. (1961). The applied science of rubber. WJS Naunton, Arnold, London, pp. 510.

Howgate, P.G., 1979. Shape Factor for Rubbers in shear and compression. Applied Science Publishers Ltd.

Kalfas, K.N., Mitoulis, S.A., Katakalos, K., 2017. Numerical study on the response of steel-laminated elastomeric bearings subjected to variable axial loads and development of local tensile stresses. Engineering Structures. Elsevier Ltd 134, 346–357. https://doi.org/10.1016/j.engstruct.2016.12.015.

Kelly, J.M., Konstantinidis, D.A. (Eds.), 2011. Mechanics of Rubber Bearings for Seismic and Vibration Isolation. Wiley.

Koh, C.G., Kelly, J.M., 1988. A simple mechanical model for elastomeric bearings used in base isolation. Int. J. Mech. Sci. 30 (12), 933–943. https://doi.org/10.1016/0020-7403(88)90075-6.

Koh, C.G., Kelly, J.M., 1989. Compression stiffness of bonded square layers of nearly incompressible material. Eng. Struct. 11 (1), 9–15. https://doi.org/10.1016/0141-0296(89)90027-8.

Koh, C.G., Lim, H.L., 2001. Analytical solution for compression stiffness of bonded rectangular layers. Int. J. Solids Struct. 38 (3), 445–455.

Kosten, C. W. (1942). Over de elastische eigenschappen van gevulcaniseerde rubber. (On the elastic properties of vulcanized rubber)," thesis presented to Delft University, Delft, Netherlands, in partial fulfillment of the requirements for the degree of Doctor of Philosophy (in Dutch).

Lanzo, A.D., 2004. On elastic beam models for stability analysis of multilayered rubber bearings. Int. J. Solids Struct. 41 (20), 5733–5757. https://doi.org/10.1016/j.ijsolstr.2004.04.024.

Lindley, P.B., 1966. Load-compression relationships of rubber units. J. Strain Anal. Eng. Design. 1, 190–195. https://doi.org/10.1243/03093247V013190.

Montuori, G.M., Mele, E., Marrazzo, G., Brandonisio, G., De Luca, A., 2016. Stability issues and pressure–shear interaction in elastomeric bearings: the primary role of the secondary shape factor. Bull. Earthq. Eng. 14 (2), 569–597.

Muhr, A. H. (2017). Lateral stiffness of rubber mounts under finite axial deformation. Constitutive Models for Rubber X - Proceedings of the 10th European Conference on Constitutive Models for Rubber, ECCMR X 2017, pp. 153–158. doi: 10.1201/9781315223278-26.

Orfeo, A., Tubaldi, E., Muhr, A.H., Losanno, D., 2022. Mechanical Behaviour of rubber bearings with low shape factor. Eng. Struct. 266, 114532.

Payne, A. R. (1962). Effect of compression on the shear modulus of rubber. I&EC Product Research and Development, 1(2), pp. 86–88. doi: 10.1021/i360002a005.

Roeder, C.W., Stanton, J.F., Taylor, A.W., 1987. Performance of Elastomeric Bearings. National Cooperative Highway Research Program Report.

Schapery, R.A., 2018. Elastomeric bearing sizing analysis Part 1: Spherical bearing. Int. J. Solid. Struct. Elsevier Ltd 152–153, 118–139. https://doi.org/10.1016/j.ijsolstr.2018.03.010.

Schapery, R.A., Skala, D.P., 1976. Elastic stability of laminated elastomeric columns. Int. J. Solids Struct. Pergamon Press 12 (6), 401–417. https://doi.org/10.1016/0020-7683(76)90018-4.

Siegenthaler, R., 1970. Earthquake proof building supporting structure with shock absorbing damping elements. Schweizerische Bauzeitung, Nr, p. 20.

Stanton, J.F., Scroggins, G., Taylor, A.W., Roeder, C.W., 1990. Stability of laminated elastomeric bearings. J. Eng. Mech. 116 (6), 1351–1371.

Thomas, A. G. (1982). The Design of Laminated Bearings I. Proceeding of the Conference on NR for Earthquake Protection of Buildings, pp. 229–246.

Timoshenko, S. P. (1921). LXVI. On the correction for shear of the differential equation for transverse vibrations of prismatic bars. The London, Edinburgh, and Dublin Philosophical Magazine and Journal of Science, 41(245), pp. 744–746. doi: 10.1080/14786442108636264.

Tsai, H.C., Lee, C.C., 1998. Compressive stiffness of elastic layers bonded between rigid plates. Int. J. Solids Struct. 35 (23), 3053–3069. https://doi.org/10.1016/S0020-7683(97)00355-7.

Wang, C.M., 1995. Timoshenko Beam-Bending Solutions in Terms of Euler-Bernoulli Solutions. J. Eng. Mech. 121 (6), 763–765.
Warn, G. (2014) 'Vertical Stiffness of Elastomeric and Lead–Rubber Seismic Isolation Bearings', 9445(July 2007). doi: 10.1061/(ASCE)0733-9445(2007)133.
Yabana, S. and Matsuda, A. (2000) 'MECHANICAL PROPERTIES OF LAMINATED RUBBER BEARINGS FOR THREE-DIMENSIONAL SEISMIC ISOLATION', 12Wcee, pp. 1–8.
Yeoh, O.H., 1985. The Compression Modulus of tall rubber cylinders. J. Rubber Res. Institute Malaysia 33 (3), 109–114.